This is to certify that the

thesis entitled

Automated System For Determining
The Acoustic Impulse Response
Of A Layered Model

presented by

Jeffrey James Giesey

has been accepted towards fulfillment
of the requirements for

Masters degree in Elect. Engr.

Major professor

Date Nov. 13, 1986

AUTOMATED SYSTEM FOR DETERMINING THE ACOUSTIC IMPULSE RESPONSE OF A LAYERED MODEL

By

Jeffrey James Giesey

A THESIS

Submitted to
Michigan State University
in partial fulfillment of the requirements
for the degree of

MASTER OF SCIENCE

Department of Electrical Engineering
and System Science

1986

ABSTRACT

AUTOMATED SYSTEM FOR DETERMINING THE ACOUSTIC IMPULSE RESPONSE OF A LAYERED MODEL

By

Jeffrey James Giesey

Present ultrasonic imaging techniques make use of only the magnitude of the receiving signal. A method was developed which gives the impedance profile of a layered material from the acoustic impulse response. In this thesis an automatic system was developed to calculate the acoustic impulse response of a layered model. The system was tested with three different transducers and two different models. Three different filtering methods were also investigated. The results showed that in most cases, the layers of the models could be seen in the impulse response by using this system. Also, the resolution of the system was greater than that of conventional ultrasonic imaging.

ACKNOWLEDGMENTS

I would like to thank L.T. Wu for his help in developing some of the software used for this thesis, and Dr. Robert Barr and Dr. H. Roland Zapp for their helpful suggestions. Finally, I thank Dr. Bong Ho, my advisor, for his guidance on this work and my education.

TABLE OF CONTENTS

Page

LIST OF TABLES

LIST OF FIGURES

Page

Page

CHAPTER 1

INTRODUCTION

Ultrasonic waves have been used to produce images in medical applications since the 1970's. Almost all imaging schemes so far have only made use of the magnitude of the returned signal. A much more useful image of an object can be produced by displaying the acoustic impedance and attenuation of that object. So far work done on impedance and attenuation imaging has been limited to a few researchers whose work involved hand digitizing the return ultrasound signal. Thus, the images done so far take more work to obtain and could not be considered a practical means of imaging. It is the goal of this project to automate the signal acquisition and signal processing to produce an acoustic impulse response from which the impedance and attenuation images can be found. This project will enable future improvements to be made in the signal processing and eventually produce a practical way to produce both acoustic impedance and attenuation images.

The basic principle behind ultrasonic imaging is to produce a pressure wave with a transducer and apply the wave to the medium to be imaged. This wave propagates through the medium until it reaches a material with a different acoustic impedance. At the boundary of these two materials, part of the wave will be transmitted through the second medium and part of the wave will be reflected back to the transducer. This reflected wave can be detected by the same transducer and displayed.

Presently, there are two types of images produced that account for the vast majority of ultrasonic images. They are called A-mode and B-mode. For an A-mode image, the return signal is envelope-detected and the amplitude is displayed on a CRT as a function of time. The acoustic signals are then translated from functions of time to functions of distance by dividing time by the speed of sound in the material. Therefore, time and distance are used interchangeably. The A-mode display is used to locate boundaries between layers of difference impedances. Applications include estimation of liver size, location of brain midline, and measurement of eye structure. For a B-mode image, the signal is envelope-detected similarly to an A-mode except it is displayed as a line of dots called pixels with the brightness of the individual pixels corresponding to the amplitude of the signal at that point. By combining many different angles of transducer orientation, a two-dimensional image is produced. B-mode imaging is most widely used in fetal monitoring and other imaging.

It is believed that a plateau has been reached using these two imaging techniques and others that use envelope detection. This plateau was reached mainly because these schemes only utilize a small portion of the returned signal. An imaging scheme was developed by J.P. Jones in which the whole signal, both magnitude and phase, was used. This method makes use of all the spectral information to determine the impedance profile of the material. This thesis extends the scheme into ultrasonic imaging.

The acoustic impedance is a measure of the pressure required to give a particle of a medium a certain velocity. For example, air has a lower acoustic impedance than water, so pressure waves travel in water much more easily than through air. An impedance image is developed by taking the input waveform and the output waveform and deconvolving them in the frequency domain to find the impulse response. The theory will be reviewed later in this thesis. The relation is:

$$\int_0^t h(\tau)\, d\tau = 1/2 \ln\, [z(t)/z_0]$$

In order to find the impulse response, we first find the incident waveform x(t) and the reflection waveform y(t). Then, we take the Fourier transform of both to get X(f). Dividing Y(f) by X(f), we obtain the frequency domain impulse response H(f). We then take the inverse Fourier transform to get the impulse response h(t) with which the impedance profile z(t) can be found. This scheme has the advantage over the present techniques in that:

1. It gives the direction of the impedance change, not just the magnitude. This scheme will tell if the boundary is between a higher to lower impedance medium or a lower to higher impedance medium.

2. It gives the value of impedance for a layer relative to the initial impedance, not just the preceeding layer. Thus, if the acoustic impedance is known for any of the layers, the acoustic impedance is known for the entire medium.

3. It greatly improves the resolution of the image because the impulses of the impedance profile are significantly narrower than those of regular envelope detection.

Another image that can be evaluated from the impulse response is the acoustic profile. Attenuation is the measure of the decrease on intensity as a pressure wave travels through a medium. In order to form the attenuation profile the medium needs to be interrogated from both sides.

The goal of this thesis is to perform the necessary data acquisition and signal processing to compute an impulse response. It is organized into four chapters. The first chapter introduces the subject and the second explains some of the theory involved in ultrasound. Chapter three describes the hardware developed to carry out the imaging and explains its operation. Chapter four presents and discusses experimental results, and is followed by suggestions for future work for the imaging system.

CHAPTER 2

THEORETICAL CONSIDERATIONS

In order to understand the project it is essential to first review some of the basic ultrasound principles. With these basic principles, we can derive the equations that relate the impulse response to the impedance profile. This section will also take a brief view of the necessary theory to do acoustic attenuation measurement, and will be followed by a discussion of the bandwidth considerations and some solutions to bandwidth problems. Finally, we will look at two ideal cases which will enable us to compare the actual experimental results with what should be expected.

2a. Review of General Ultrasound Principles

As noted before, an ultrasound image is created by sending a pressure wave into a medium. When this pressure wave reaches a change in material, part of it is reflected back and part of it is transmitted through the medium. Mathematically, the wave can be expressed with a standard wave equation describing the pressure at a particular point and time.

$$\nabla^2 p(x,t) = \rho/k \frac{d^2 p}{d t^2}$$

where p = pressure, ρ= density of the material, k =

wavenumber with $k = \omega c$, c = wave velocity, and ω = radian frequency.

The solution to the equation is of the form

$$p(x,t) = p_0 \exp[-j(\omega t - kx)]$$

The amplitude of the pressure at a given point is

$$p(x) = p_0 \exp(-\alpha x)$$

where α = attenuation constant

From the continuity equation

$$\nabla \cdot \rho u + \frac{dp}{dt} = 0$$

where u = the particle velocity and the density is relatively constant we find that

$$\nabla \cdot u + 1/k \frac{dp}{dt} = 0$$

This gives us the relation

$$-\frac{dp}{dx} = \rho \frac{du}{dt}$$

so if

$$\frac{d}{dx} \rightarrow -jx \qquad \frac{d}{dt} \rightarrow j\omega$$

we get

$$p = \rho c u$$

where $c = \omega/k$ = the velocity of propagation of the ultrasound wave

If we define $z = \rho c$ as the acoustic impedance of the material we get the handy form of

$$p = zu$$

relating the particle velocity to the pressure.

The intensity of the wave is derived from the kinetic energy

$$KE = 1/2\ \rho u^2$$

since

$$I = \frac{dE}{dt} = (KE)c$$

where I is the intensity. So

$$I = 1/2\ \rho c u^2$$

and the amplitude of the wave at a point is described by

$$I(x) = I_0 \exp(-2\alpha x)$$

When the wave reaches a boundary, part is reflected and part is transmitted. By using the boundary conditions

$$p_i + p_r = p_t$$

and

$$v_i \cos\theta_i - v_r \cos\theta_r = v_t \cos\theta_t$$

where

P_i = acoustic pressure of the incident wave

P_r = acoustic pressure of the reflected wave

P_t = acoustic pressure of the transmitted wave

V_i = particle velocity of the incident wave

V_r = particle velocity of the reflected wave

V_t = particle velocity of the transmitted wave

θ_i = angle of incident wave

θ_r = angle of reflected wave

θ_t = angle of transmitted wave

(see Figure 1)

and Snell's law, we can find the reflection coefficient (the ration of the reflected pressure over the incident

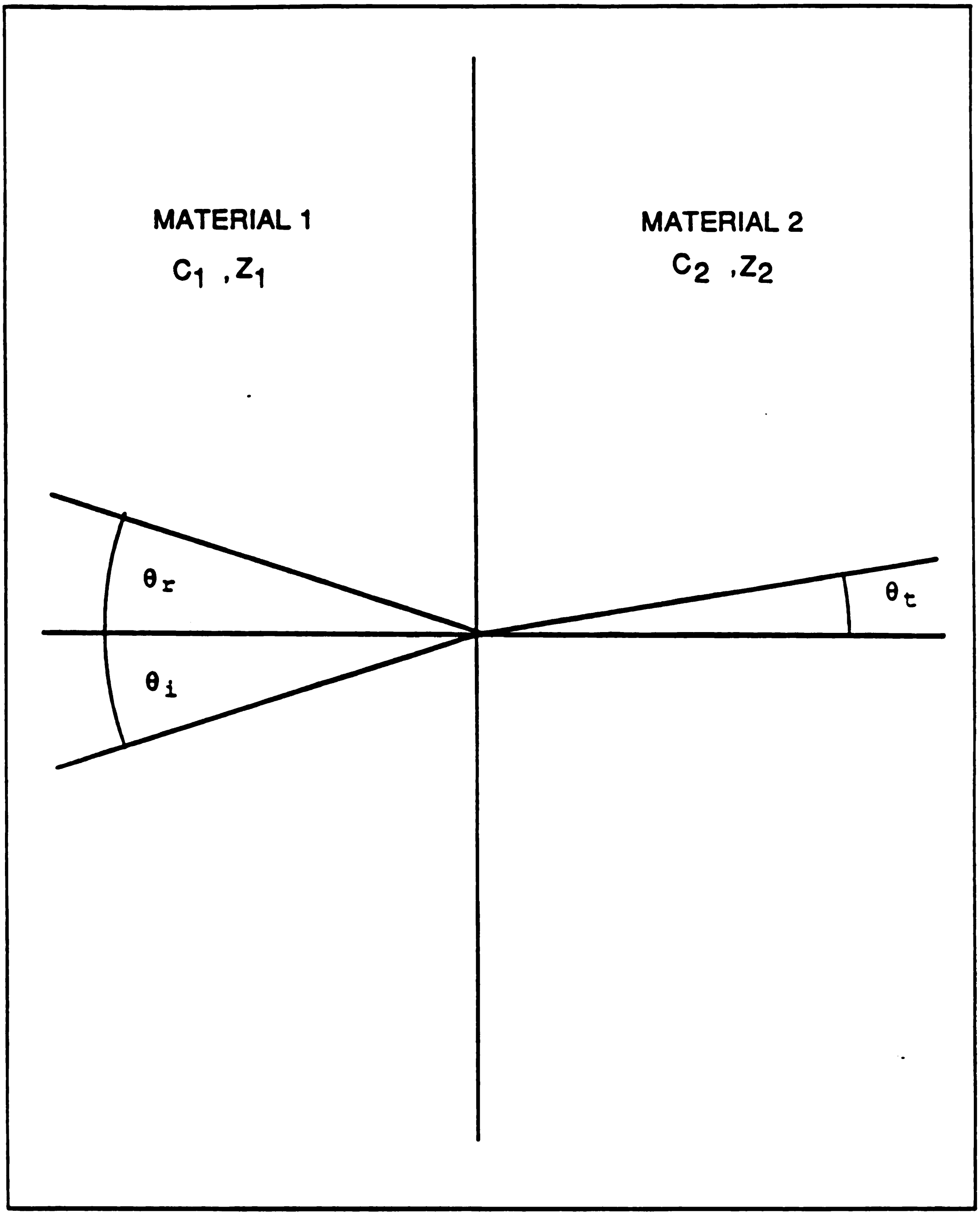

Figure 1: Definition of Variables

pressure) and the transmission coefficient (pressure over the incident pressure). If the incident wave is moving perpendicular to the surface, the reflection coefficient simplifies to

$$r = (z_j - z_i)/(z_j + z_i) \qquad (1)$$

and the transmission coefficient simplifies to

$$= 2z_j/(z_j + z_i) \qquad (2)$$

where

z_i = acoustic impedance of the first material

z_j = acoustic impedance of the second material

the intensity of the wave is proportional to the square of the pressure divided by the impedance so the intensity reflection and transmission coefficients are equal to the square of the pressure coefficients times the ratio of the impedances. This gives the reflection coefficient

$$R = (z_j - z_i)^2 / (z_j + z_i)^2$$

the transmission coefficient

$$T = 4z_j \cdot z_i / (z_j + z_i)^2$$

They are related to

$$T = (R + 1)$$

The other general aspect of ultrasound waves that is important to this thesis is the resolution of the standard techniques. For envelope detection the resolution is generally accepted to be equal to the wavelength in the best case. To get an estimate of this, a 1.00 MHz wave propagating through liver tissue (with velocity of propagation = 1545 m/s) would have a resolution of only = c/f = 1.5 mm. It is because of this poor resolution that ultrasound is not suitable for many applications.

2b. Impedance Derivation

Biological tissue is normally acoustically complex, however there is some order to it. The macro structure of the tissue suggests a multi-layered, nonplanar, laminated structure. Since the lateral variations in material can be reduced by focusing the transducer to a desired depth, it is fairly safe to use a planar, multilayered structure to test the system. However the following assumptions must be made: 1. Only first order reflections are used. 2. Each layer is homogeneous (i.e. constant impedance in layer). 3. The boundary between layers is small compared to the layer itself. 4. There are no large differences in impedance (i.e. small reflections). The following terms must be defined:

$x(t)$ = input waveform

$y(t)$ = output waveform

$X(\omega)$ = frequency spectrum of input

$Y(\omega)$ = frequency spectrum of output

$H(\omega)$ = frequency spectrum of impulse response

$h(t)$ = impulse response

z_n = acoustic impedance of the n^{th} layer

r_n = reflection coefficient at the n^{th} boundary

(see Figure 2)

The derivation of the relation between the impedance profile and the impulse response is as follows. The impulse response will be the sum of all the reflections from the various boundaries. Neglecting attenuation we can see from Figure 2 that:

$$h(t) = \sum_{n=1}^{m} a_n \delta(t - t_n) \quad (3)$$

and

$$a_1 = R_1$$

$$a_2 = (R_1 + 1) \; R_2 \, (R_1 - 1)$$

$$a_3 = (R_1 + 1)(R_2 + 1) R_3 (R_1 - 1)(R_2 - 1)$$

so

$$a_n = R_n \prod_{i=1}^{n-1} (1 - R_i^2)$$

putting this into equation 3, we get

$$h(t) = \sum_{n=1}^{m} R_n \prod_{i=1}^{n-1} (1 - R_i^2) \quad \delta(t - t_n)$$

or

$$h(t_n) = R_n \prod_{i=1}^{n-1} (1 - R_i^2)$$

The ratio of two successive reflections n and n + 1 equals

$$\frac{h(t_n)}{h(t_{n+1})} = \frac{R_n \prod_{i=1}^{n-1} (1 - R_i^2)}{R_{n+1} \prod_{i=1}^{n} (1 - R_i^2)} = \frac{R_n}{R_{n+1} \, (1 - R_n^2)} \quad (4)$$

taking the natural logarithm of both sides

$$\ln \left[\frac{h(t_n)}{h(t_{n+1})} \right] = \ln \left[\frac{R_n}{R_{n+1} \, (1 - R_i^2)} \right]$$

or

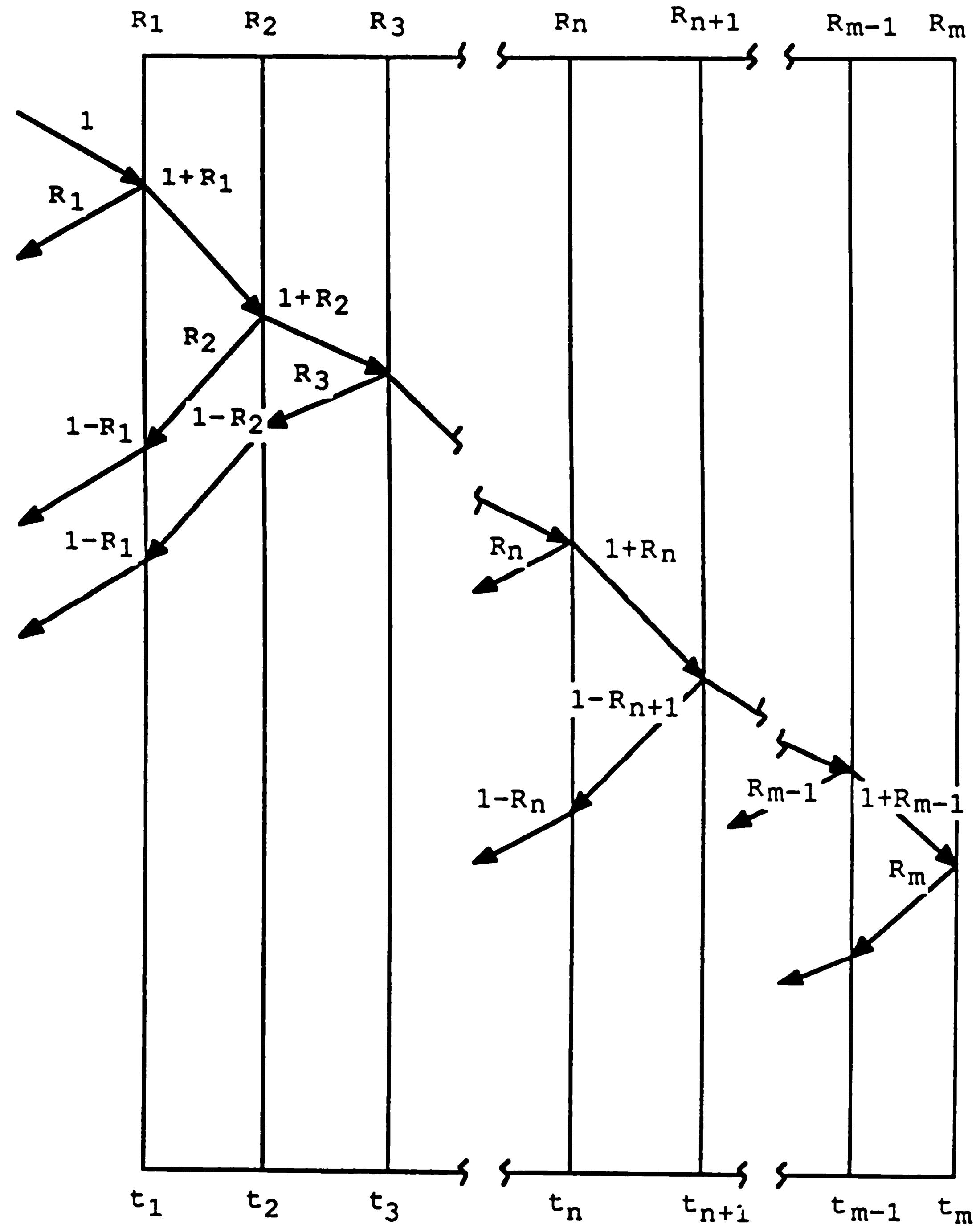

Figure 2: Determination of the Impulse Response

$$\ln[h(t_n)] - \ln[h(t_{n+1})] = \ln(R_n) - \ln(R_{n+1}) - \ln(1-R_n^2) \quad (5)$$

Rearranging equation 1, we can find

$$\frac{z_n}{z_{n+1}} = \frac{1 + R_n}{1 - R_n}$$

or

$$\ln(z_n) - \ln(z_{n+1}) = \ln(1 + R_n) - \ln(1 - R_n) \quad (6)$$

As we make this model continuous, r_n gets small so

$$\ln(z_n) - \ln(z_{n+1}) = 2R_n$$

or

$$R_n = 1/2\ [\ln(z_n) - \ln(z_{n+1})] \quad (7)$$

since

$$\lim_{x \to 0} \ln(1 + X) = X$$

Approximating

$$\ln(1 - R_n^2)$$

by

$$R_n^2$$

and substituting 7 into equation 5, we get

$$\begin{aligned} \ln[h(t_n)]-\ln[h(t_{n+1})] = \\ &\ln\Big(1/2\big[\ln[z(t_n)] - \ln[z(t_{n+1})]\big]\Big) \\ &- \ln\Big(1/2\big[\ln[z(t_{n+1})] - \ln[z(t_{n+2})]\big]\Big) \\ &- 1/4\big[\ln[z(t_n)] - \ln[z(t_{n+1})]\big] \end{aligned}$$

calling $t_n - t_{n+1} = \Delta t$

$$\begin{aligned} \Delta t\left[\frac{\ln[h(t)]-\ln[h(t+\Delta t)]}{\Delta t}\right] = \\ &\ln\left[1/2\ \frac{[\ln[z(t)] - \ln[z(t+\Delta t)]]}{\Delta t}\right] \\ &-\ln\left[1/2\ \frac{[\ln[2(t+\Delta t)] - \ln[z(t+2\Delta t)]]}{\Delta t}\right] \end{aligned}$$

$$- 1/4\ \Delta t^2 \left[\frac{\ln[z(t)] - \ln[2(t+\Delta t)]}{\Delta t}\right]^2$$

By the definition of the derivative

$$\Delta t \cdot \frac{d}{dt}\left[\ln[h(t)]\right]_{t=t_n} = \ln\frac{d}{dt}[1/2\ln[z(t)]]\Big|_{t=t_n} - \ln\frac{d}{dt}\left[1/2\ \ln\ [z(t)]\right]\Big|_{t=t_{n+1}} - 1/4\ \Delta t^2 \left[\frac{d}{dt}\ln[z(t)]\right]^2\Big|_{t=t_n}$$

Rearranging and taking the definition of the derivative again

$$\frac{d}{dt}\left[\ln[h(t)]\right] = \frac{d}{dt}\left[\ln\left[\frac{d}{dt}[1/2\ln[z(t)]]\right]\right] - 1/4\ \Delta t\left[\frac{d}{dt}\ln[z(t)]\right]^2$$

integrating both sides

$$\ln[h(t)] = 1/2\ \frac{d}{dt}\ \ln[z(t)] - 1/4 \cdot \Delta t \cdot \int \left[\frac{d}{dt}\ln[z(t)]\right]^2$$

as Δt approaches zero

$$1/4\ \Delta t \int \left[\frac{d}{dt}\ln[z(t)]\right]^2 = 0$$

so put in a better form is

$$\int_0^t h(\tau) = 1/2\ \ \ln[z(t)]$$

2c. Attenuation Imaging

In some instances tissues will have a small difference in acoustic impedance but a large difference in their acoustic attenuation. For example, the impedance difference between white and gray brain matter is less than .1% whereas the difference in attenuation is two orders of magnitude. If attenuation is taken into consideration, equation 8 becomes

$$h(t) = 1/2 \exp\left(- \int_0^t \alpha(t)\,dt \right) \frac{d}{dt} \ln[z(t)]$$

If the medium is interrogated from both sides, as shown by Jayasumana, the attenuation variation along the medium can be found from the following relation

$$\ln[z(t)/z(0)] = \exp\left(- \int_0^t \alpha(t)\,dt \right) \int_0^t [-4h_1(t)\,h_2(T - t)]^{1/2} dt$$

where

$h_1(t)$ = impulse response of the medium when interrogated from the right

$h_2(t)$ = impulse response of the medium when interrogated from the left

$z(t)$ = impedance profile

$z(0)$ = initial impedance

$\alpha(t)$ = attenuation profile

(see Figure 3)

2d. Bandwidth Considerations

Under ideal conditions we should be able to find $H(\omega)$ and thus find $h(t)$ measuring $x(t)$ and $y(t)$. In principle we are assured that this is correct, but in practice problems arise because of the unreliability of $H(\omega)$ outside bandwidth of the input signal (see Figure 4). In order to correct this there are two options. The first is to try to restore the frequency components outside the range f1, f2 by iterative techniques. This was successfully done by Papoulis and Beretsky. The other solution is to severely limit the components of $H(\omega)$ outside the range of f1, f2 by the use of a suitable window. The latter of the two above methods was chosen for this thesis because of its ease of implementation.

The actual waveform is $H(\omega)$, but because of the presence of noise the waveform $H_o(\omega)$ is recorded, $H_o(\omega)$ is composed of the original signal and noise

$$H_o(\omega) = H(\omega) + n(\omega)$$

where $n(\omega)$ = noise spectrum.

To eliminate the noise, $H_o(\omega)$ is multiplied by a window function $w(\omega)$ which passes frequencies in the range f1, f2 but greatly diminishes those outside that range. Because the signal should be significantly greater than the noise inside the range f1, f2 the new spectrum

$$H'_o(\omega) = w(\omega) \quad H_o(\omega).$$

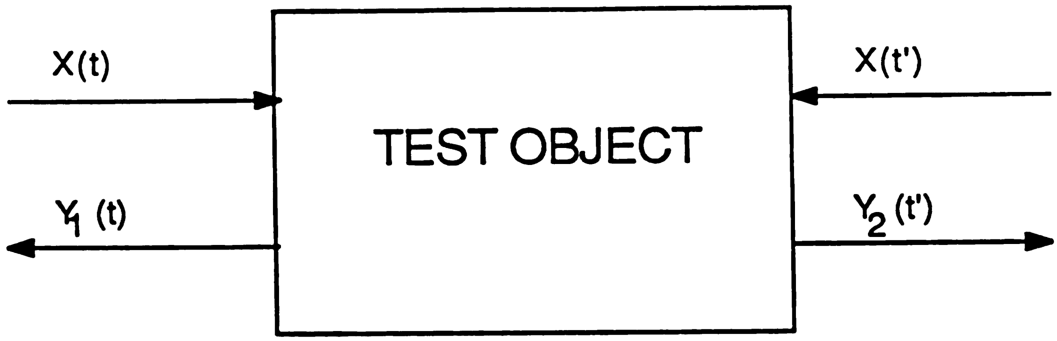

Figure 3: Bidirectional Interrogation

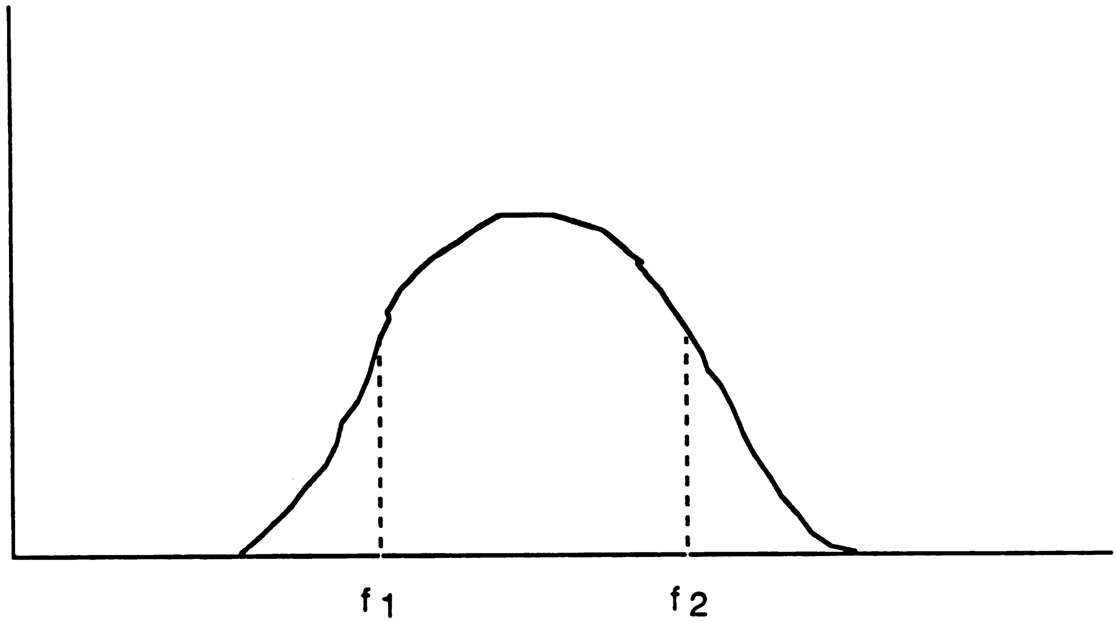

Figure 4: Typical Frequency Spectrum of Input Signal

should closely resemble the original spectrum $H_o(\omega)$. It is with $H_o(\omega)$ that the impulse response h(t) is evaluated.

2e. Ideal Cases

In order to know what to expect and to properly analyze the experimental results it is important to explore two ideal cases. The start of the ideal case is the model shown in Figure 5. It is a model similar to the actual ones used in the experiments. The impedance profile for this model will look something like Figure 6. Using the equation

$$h(t) = 1/2 \frac{d}{dt} \ln[z(t)]$$

the evaluation impulse response is shown in Figure 7. Taking the inverse Fourier transform of h(t) the spectrum is shown in Figure 8 which is simply an offset sinusoidal wave.

Using the same model and impedance profile, we change the shape of h(t) to be less ideal than in the first case. This new h(t) is shown in Figure 9. The $H(\omega)$ evaluation from this is shown in Figure 10. Notice that it is similar to Figure 8 but is multiplied by a sinc squared function. As the spikes of h(t) get narrower the main lobe of the sinc squared function gets wider and we approach the first case.

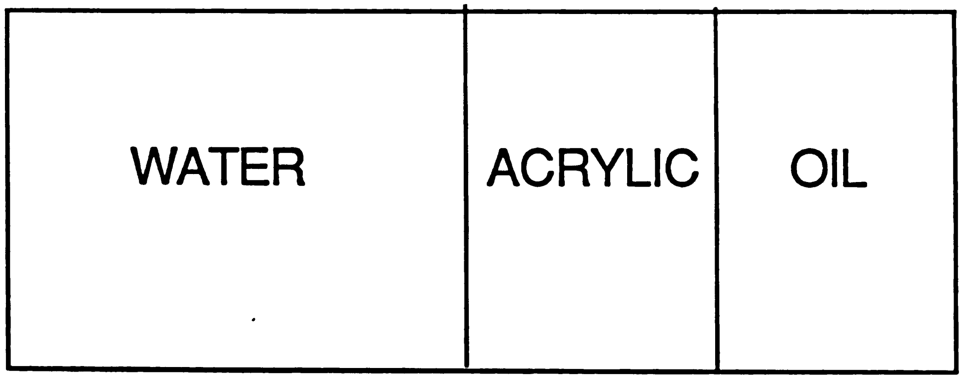

Figure 5: Ideal Model

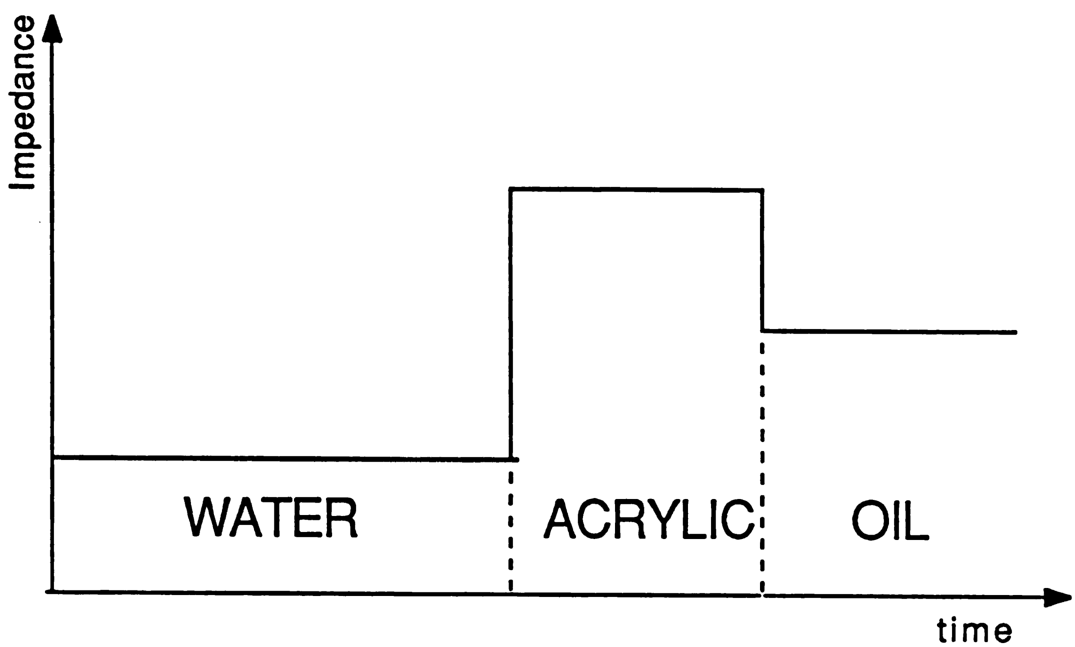

Figure 6: Ideal Impedance Profile

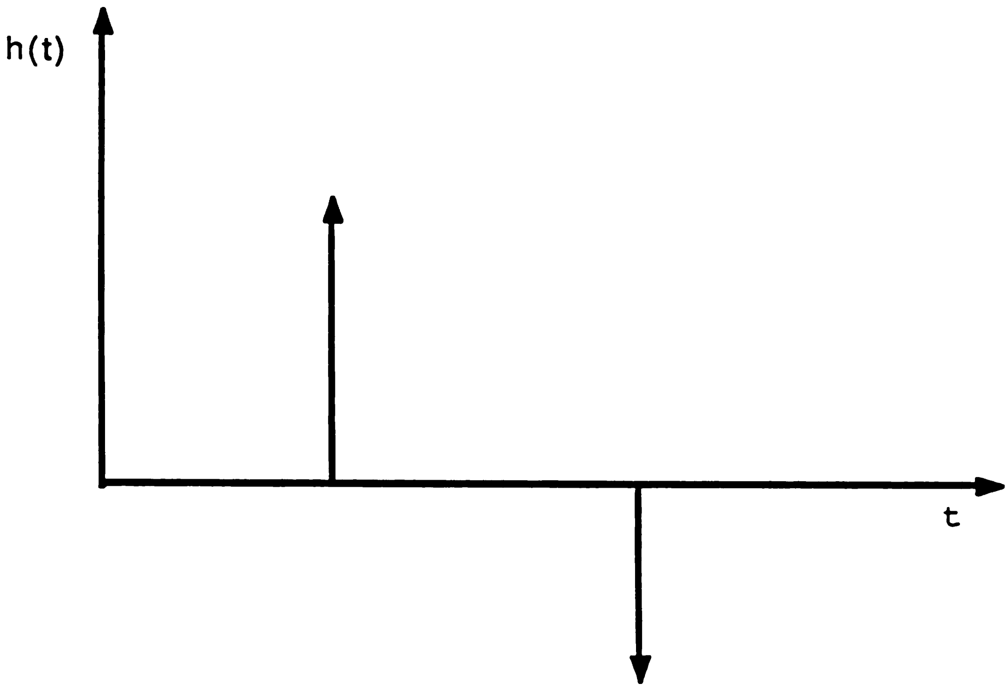

Figure 7: Ideal Impulse Response

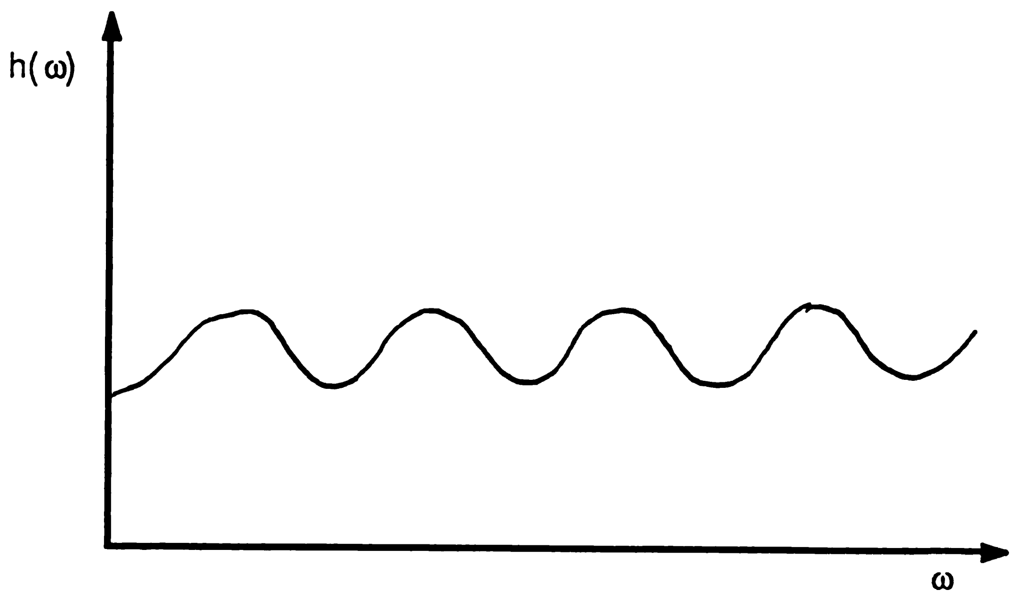

Figure 8: Spectrum of Figure 7

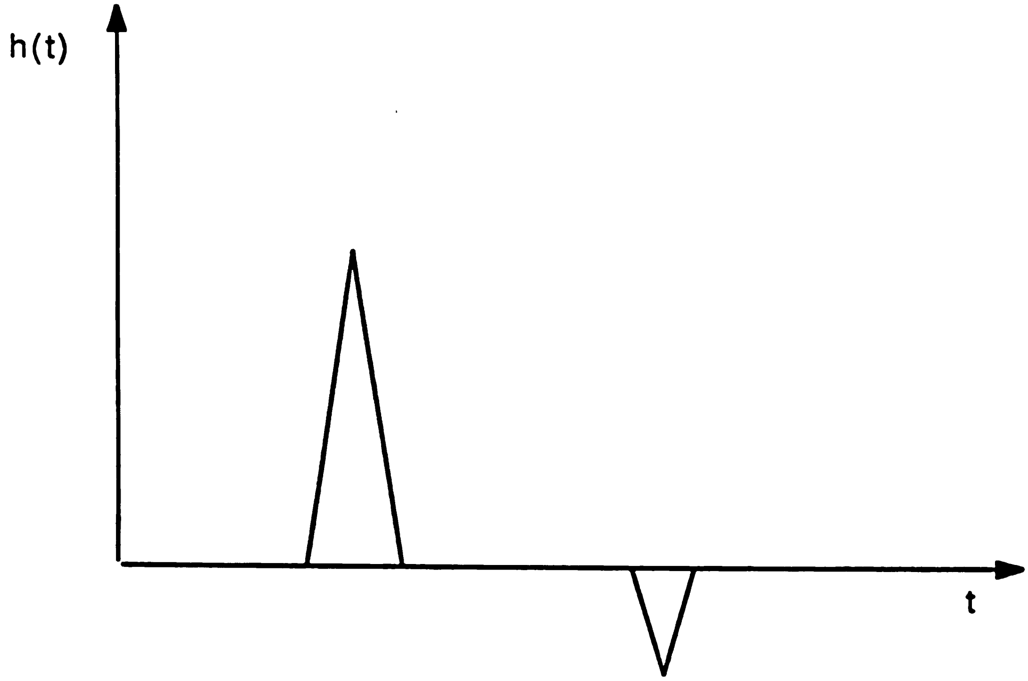

Figure 9: Less Than Ideal Response

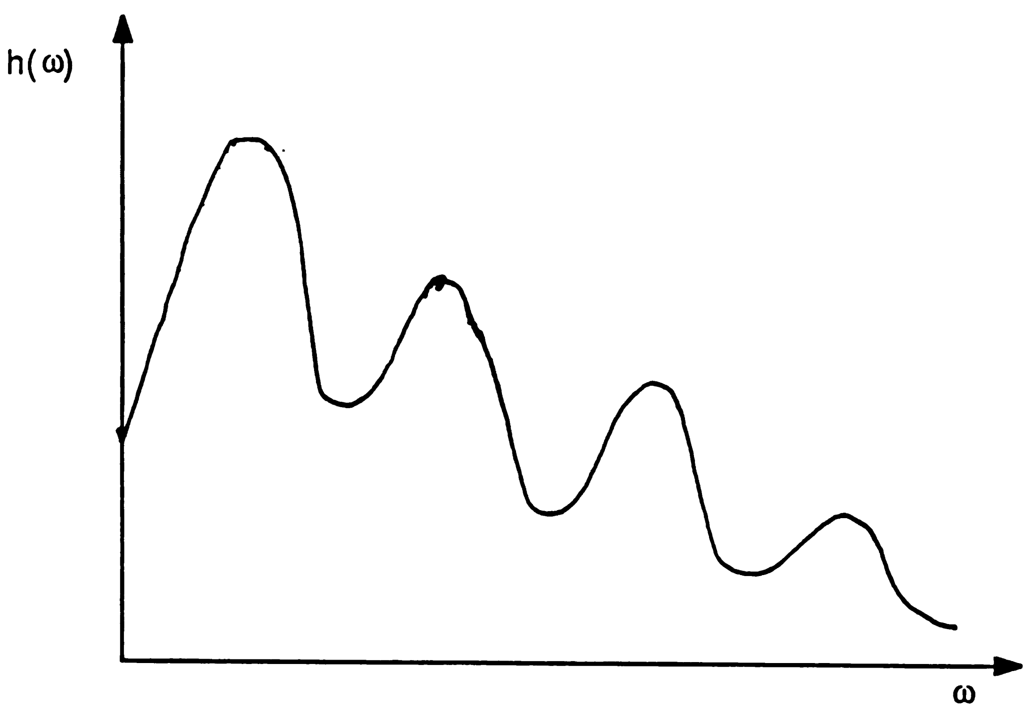

Figure 10: Spectrum of Figure 9

CHAPTER 3

SYSTEM HARDWARE

3a. Introduction

The system hardware will be discussed in this chapter. Specifically, the specifications, design, operation, and any special features will be described for the various components of the system. The parts are the microcomputer, bus buffer, range gate, A/D converter board, and the pulser/receiver.

Figure 11 shows a block diagram of the system. The sampling process is initiated by the computer when it sends an impulse through the bus buffer to the range gate. This signal is immediately passed on to the pulser/receiver which sends a pulse to the transducer. The same signal is also delayed and then sent to the A/D board to start the conversion process. The A/D board samples and stores the signal from the pulser/receiver. Finally the digitized signal is sent asynchronously to the computer through the bus buffer and is stored on a disk.

3b. Computer

The computer controls the entire system and is the most important link in making the system automated. The

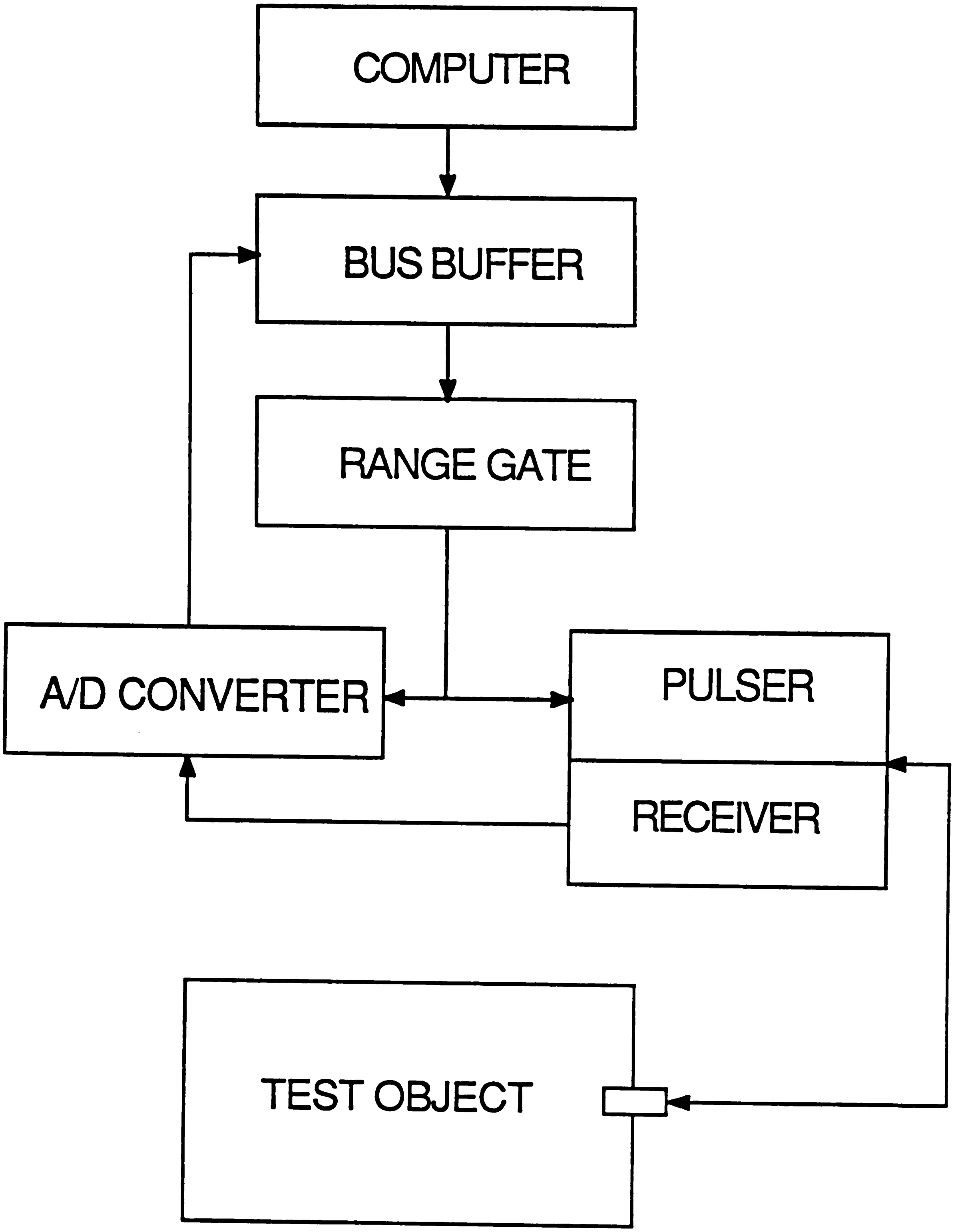

Figure 11: System Diagram

computer used was the Cromemco Z-2 with dual disk drive, and I/O card. The Cromemco contains the Z-80 microprocessor so all assembly language programs were written with Z-80 instructions.

The most important aspects of the computer to the project are the input-output features. Figure 12 shows the basic timing diagram for both the read and write cycles. Of special interest is the read cycle. The simplest and fastest read instruction to use is the INIR instruction. In this instruction, the C register contains the read address, the HL register stores the initial memory location to use, and the B register contains the number of samples to be read. The INIR instruction puts the address on the address bus, and releases the address bus. The instruction then increments HL, decrements B, and continues to repeat the entire process until the B register contains zero.

The WAIT line is also of interest. When this line is brought low, the microprocessor will halt activity until the line returns to high. The asynchronous data transmission is controlled by this line.

3c. Bus Buffer

The bus buffer controls the input and output of the computer and its relation to the other components of the system. It also takes the addresses from the computer and

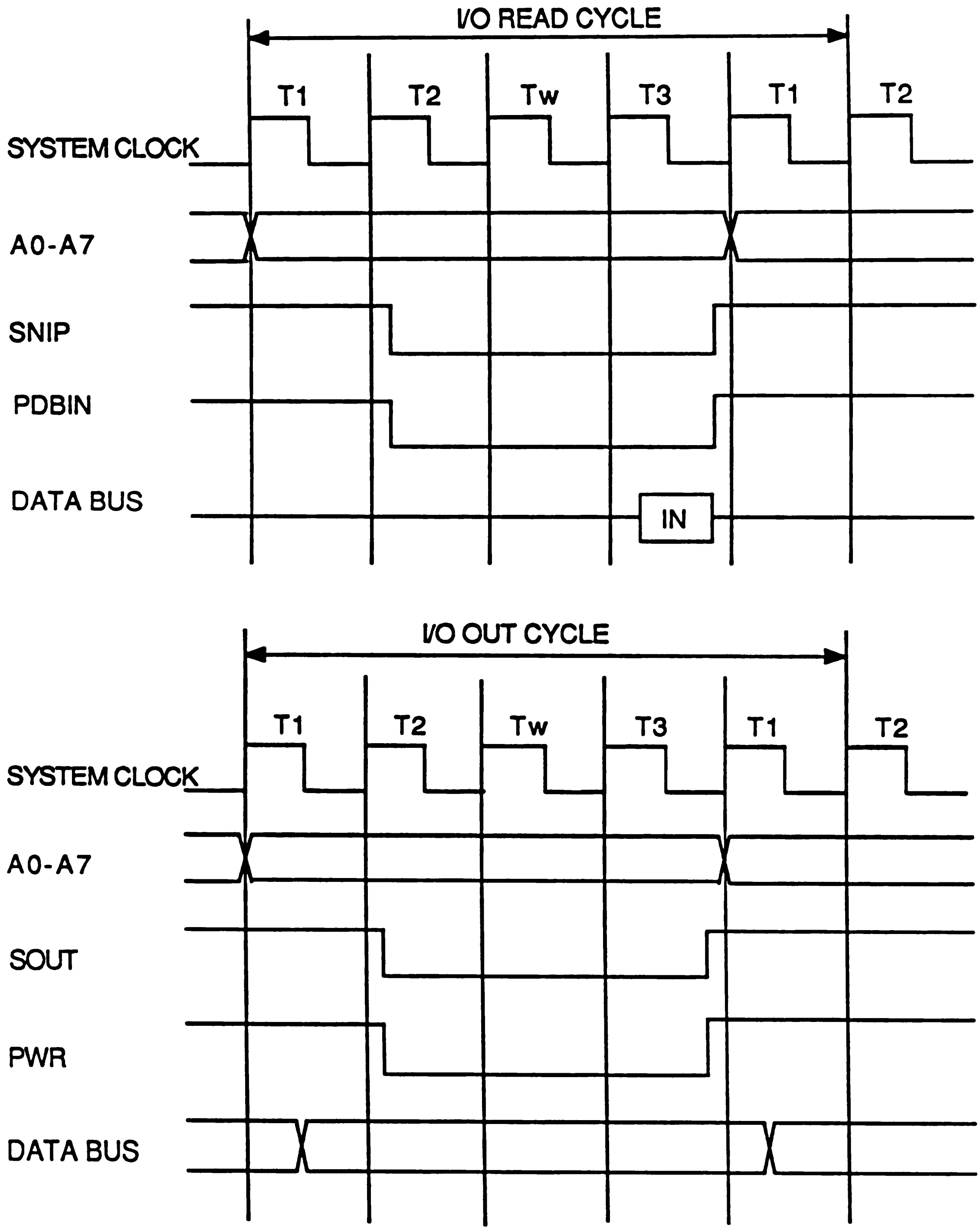

Figure 12: Input and Output Timing Diagram

turns them into control signals that are in turn used by the system components. Figure 13 shows a diagram of the bus buffer. One signal needed is the start signal which goes to the range gate and initiates the process. The other signal needed is a data-received signal which goes to the A/D board and tells it when the computer has received the data byte.

The bus buffer board accomplishes its task quite simply. It contains two different decoders for the addresses. It is from the input decoder that the START signal is taken from address 13H and the WRITE DONE signal from address 12H. The bus buffer takes the "and" of the SINP and PDBIN signals to enable the input decoder, and the "and" of the SOUT and PWR signals to enable the output decoder.

3d. Range Gate Controller

The function of the range gate controller is to enable the system to monitor the return from a specified depth so that the desired area can be examined without using extensive memory space and signal processing time. The range gate controller is shown in Figure 14. The range gate is basically a count-down counter, which triggers the A/D converter to start on the zero count. The initial

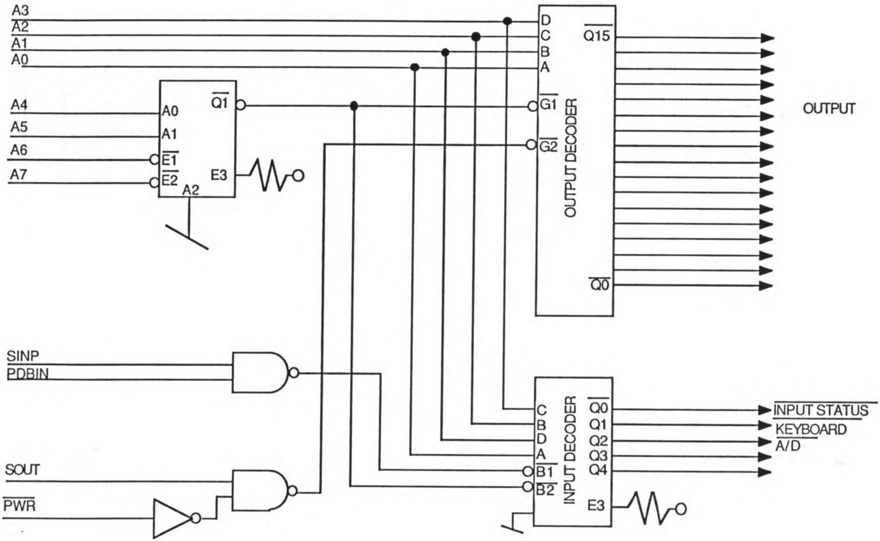

Figure 13: Bus Buffer

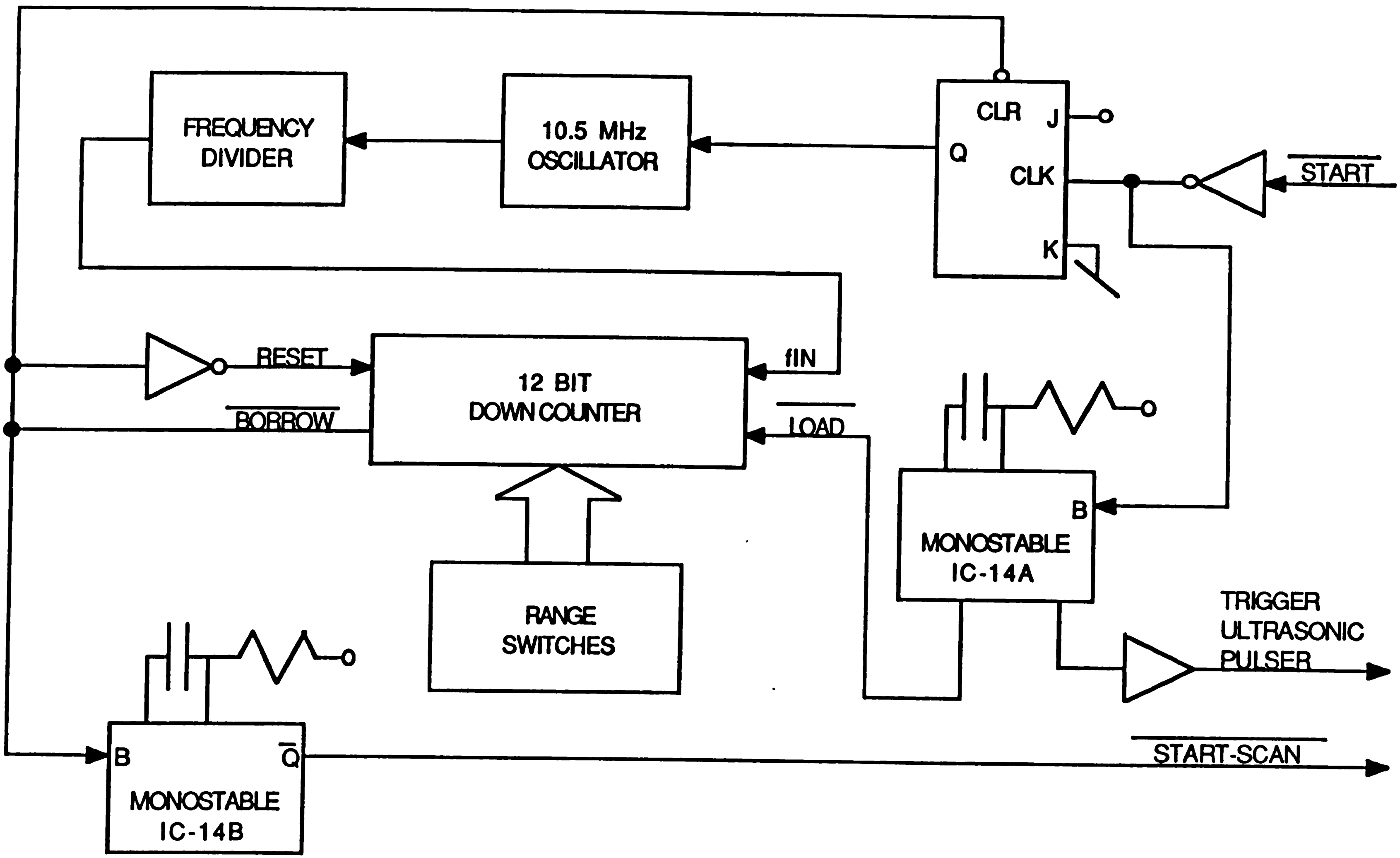

Figure 14: Range Gate Controller

value in the counter is set by switches in a separate control box. The range gate has a 10.5 MHz clock divided by 10 to give a counting rate of about 1 MHz. Using an average propagation velocity of 1550 m/s, this gives the round trip travel distance of 1.5 mm per count on the range gate.

The gate is initialized by a low on the START pulse which causes a monostable (IC-14A) to fire a pulse. This pulse loads the count into the counter and also sets a J-K flip-flop which starts the crystal oscillator. In addition to this the pulse is passed on to the pulser/receiver and triggers an output there. When the count reaches zero, the BORROW line goes low, which clears the flip-flop. This stops the oscillator and triggers another monostable to send a START SAMPLING signal to the A/D converter.

3e. A/D Conversion Board

The design of the A/D conversion board was the biggest challenge of the project because of the unique criteria required. Figure 15 shows a schematic of the board. Transducers with bandwidths of 1.00 MHz and 2.25 MHz were used, so according to the Nyquist criteria a sampling rate of at least 5MHz was needed. However, in order to obtain enough points to construct the impedance profile, sampling

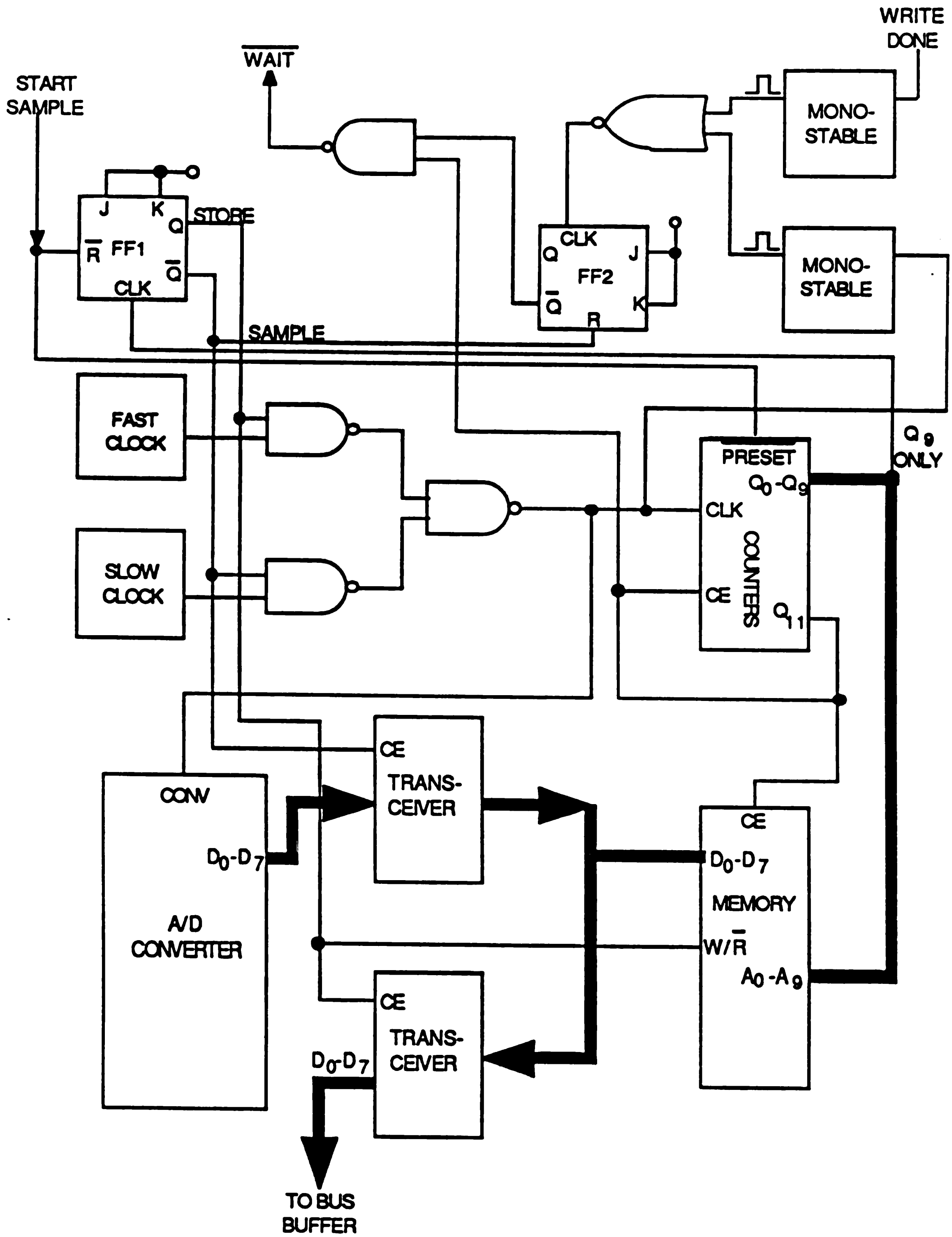

Figure 15: A/D Conversion Board

rates of over 10MHz were needed. A problem with this occurs because the INIR instruction operates at a range of around 100KHz. The A/D counter must therefore send the data to the computer at this rate or slower. In addition, the board must transmit the data to the computer asynchronously so it must handle the handshaking between them. Finally, it was desired to be able to monitor a distance of about 10 cm. At a 14.67 MHz sampling rate this corresponds to approximately 1000 samples.

The heart of this system is a TRW TDC 1048 monolithic video A/D converter. This converter is capable of sampling at rates up to 20 MHz, which is sufficient to sample the signal accurately. In order to slow down the data for the computer, the system first stored the fast sampled data into two 1024x 4 memories (2114). There is a counter that counts up twice; the first time fast to address the data storage and the second time slowly to address the writing.

The process is started by a low pulse on START SAMPLE from the range gate, which resets the flip-flop (FF1) and presets the three presettable counters (74191). The flip-flop controls whether the converter is in SAMPLE (Q) or STORE (Q) mode. When SAMPLE is set first, the fast clock (14.67 MHz) is enabled, the transceivers are set to read data from the A/D, and the memory is enabled to read. The three counters are connected to operate synchronously with 4095 values possible on lines Q_{11}-Q_0. Q_{11} is used as the system enable and is preset high with START SAMPLE. All the other lines are preset low. Q_{11} enables the counter and the memory. When the counter is enabled, it begins addressing the memory, which stores the samples from the A/D that are being converted at the same rate. Q_9-Q_0 start and 0 and count up to 1023. At 1024, Q_7 makes a high to low transition that is tied to the clock of FF1. This causes STORE to be enabled and disables SAMPLE. STORE then enables the slower clock (75 KHz), switches the transceivers to send data to the computer, and enables the memory to write.

The STORE sequence is quite a bit more complicated than the sample sequence due to the need for asynchronous data transmissions. Since the A/D board is running slower than the INIR instruction when it is in STORE mode, it is necessary to hold the computer until the next byte is ready to go to the computer. This is controlled by the WAIT line. The WAIT line is "nanded" with the system enable (Q_{11}) so that a wait can only occur when the system is running. The other input to the nand is the output of the flip-flop (FF2). FF2 is held at reset while the system is in SAMPLE mode so no points will be read at that time. The clock and the WRITE DONE are both sent into multistables (74123) and then "nored" to run the clock on FF2. Since the addresses are changed on the falling edge of the clock, the WAIT signal is disabled on the rising edge of the clock and is enabled when WRITE DONE goes low. The timing diagram for this process is shown in Figure 16. This process is continued as 0_9-Q_0 go from 0 to 1023 again but this time Q_{10} is set. At 1024, Q_{11} goes low and turns off the system.

3f. Ultrasonic Pulser/Receiver

The pulser/receiver used by this system is the Panametric 5050PR, which performs two functions. First it applies a high voltage pulse to the piezo-electric transducer which in turn produces the pressure wave. Secondly, it receives the electrical signal from the transducer after it receives the return wave.

The 5050PR can be controlled two different ways. The first is the trigger mode where the device will emit a single pulse when triggered. This is the mode that was used for data acquisition with this system. The other mode is repeat mode where the pulser fires at an adjustable rate from 200- 500 kHz. This mode was to observe the output wave form and adjust it for an optimal signal. The adjustments available were 0, 20, or 40 dB of input attenuation, four pulse energy levels, and a variable damping adjustment.

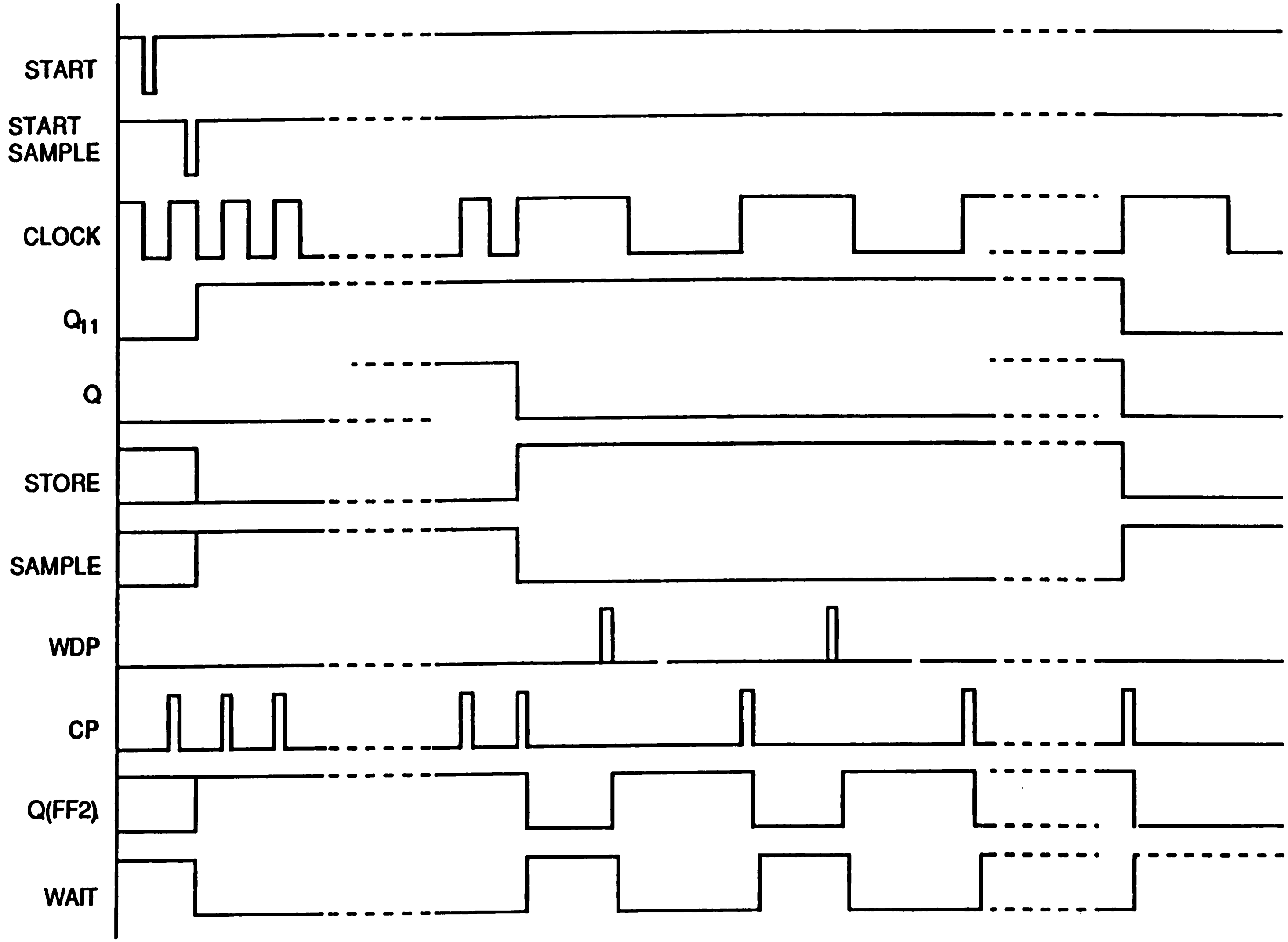

Figure 16: Data Transfer Timing Diagram

CHAPTER 4

EXPERIMENTAL RESULTS AND FUTURE POSSIBILITIES

4a. Introduction

This chapter will first explain the system set-up and the data collection process. Next, it will discuss the types of experiments done, the results of those experiments, and an explanation of the results. Finally, it will explore the future possibilities of the system.

4b. Data Acquisition

The system set-up is shown in Figures 17 and 18. The input waveform x(t) is found by reflecting the incident signal off a water-to-air interface. We can be assured that this is the actual input because there is total reflection from this interface. The acoustic impedance of water is about 3700 times that of air so the reflection coefficient is 1. The output signal y(t) was the waveform reflected from the models and received by the transducer.

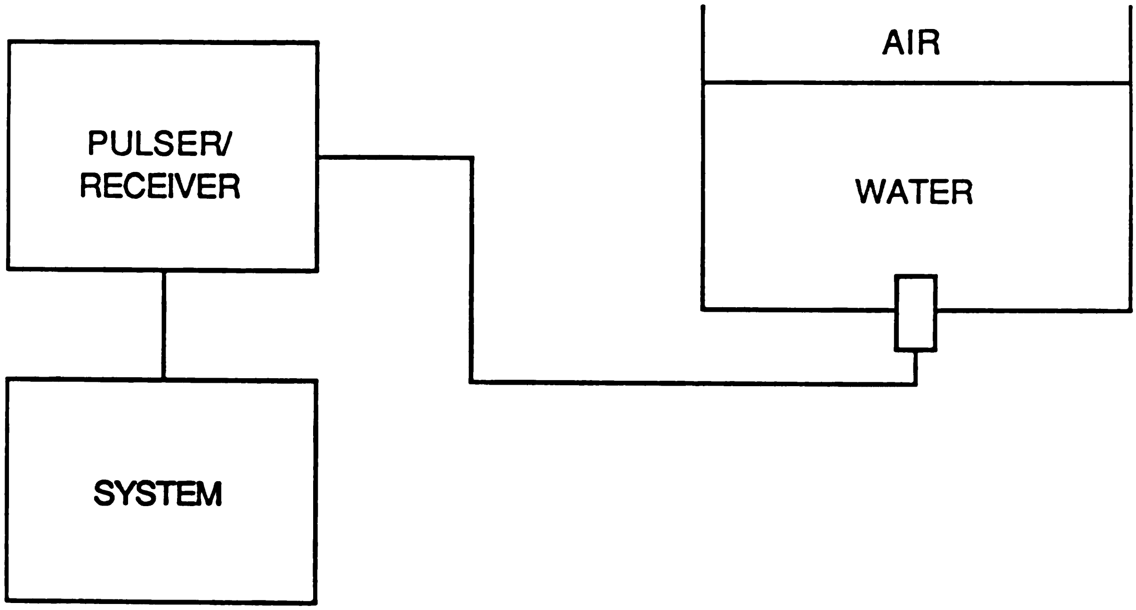

Figure 17: Waveform X(t) Recording

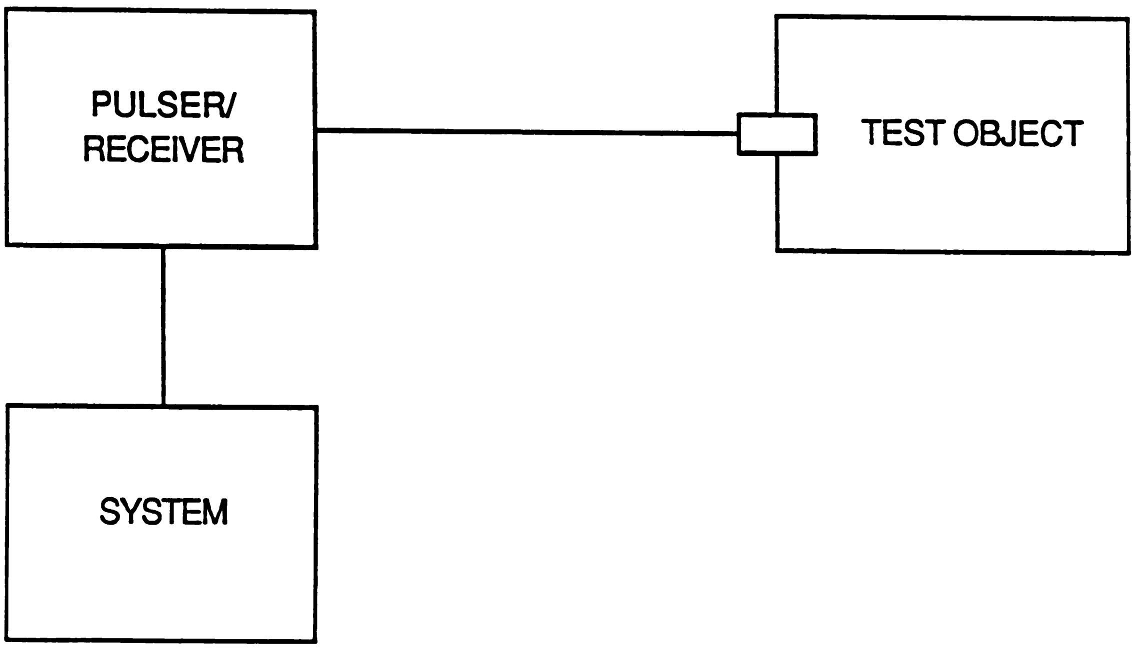

Figure 18: Waveform Y(t) Recording

The experimental procedure follows:

1. Put transducer in water to air interface, record waveform x(t), and store on disk.
2. Put transducer in model, record waveform y(t), and store on disk.
3. Send x(t) and y(t) to Cyber 750 using utility program.
4. Evaluate X(f), Y(f), H(f) and h(t) on the Cyber.

4c. Experimental Results

The experiments were selected to test a range of conditions and signal processing schemes. Two different models, three different transducers, and three different signal processing algorithms were used. The two models are shown in Figure 19 and 20. Model 1 was designed to test the system in cases of wide spaces between the layers. Model 2 was designed to test smaller boundaries and get some idea of the resolution of system. The three transducers used were a 1.00 MHz focused transducer, a 2.25 MHz focused transducer, and a 2.25 MHz unfocused transducer. Comparing the 1.00 MHz and 2.25 MHz transducers should give an indication of bandwidth differences and the amount of samples needed to describe a signal. Comparing the focused and the unfocused signals should indicate if focusing makes any difference. Finally, the different

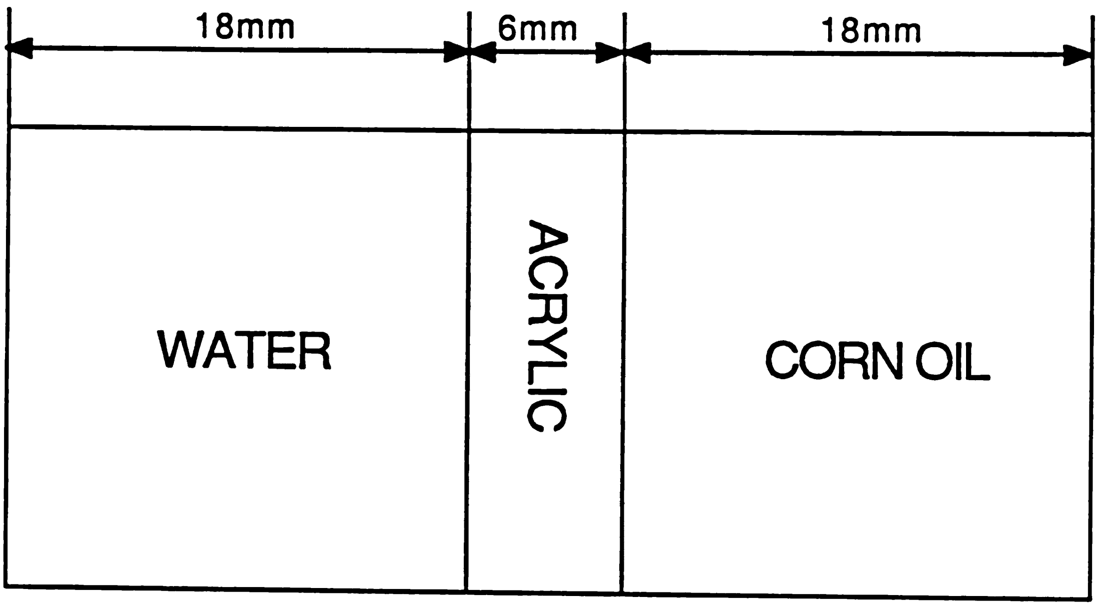

Figure 19: Model 1

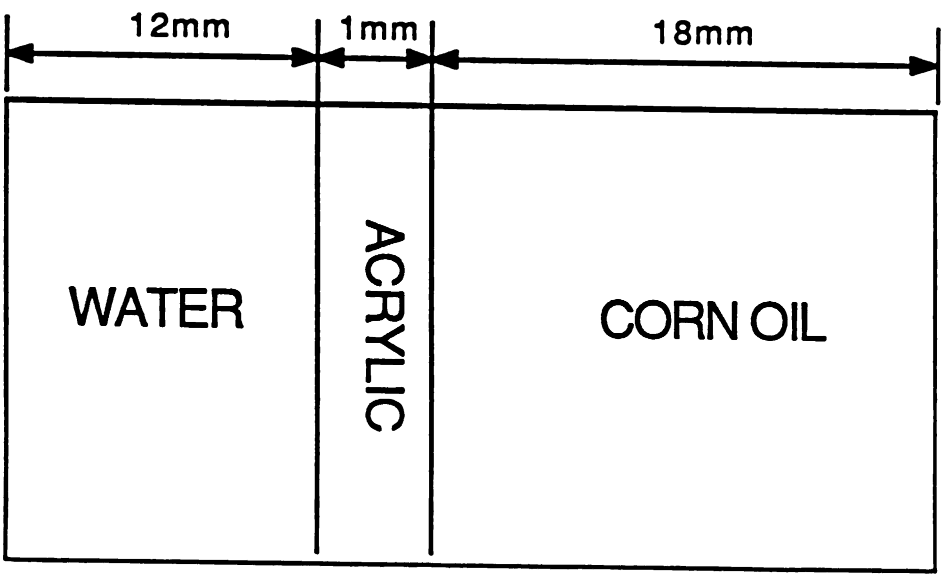

Figure 20: Model 2

signal processing schemes tried were no filtering, a simple low pass filter, and single peak detection. The simple filter used an averaging scheme $x(n) = (x(n-1)+x(n)+x(n+1))/3$ and ignored signals that were under a set threshold. The result was a wave form that was zero at all places except where there was a reflection. The single peak detection was done manually by eliminating all signals except the single peak of the reflection.

As an extensive amount of data was collected, only selected portions of it will be presented here. Figure 21 shows the typical input x(t) of the 1.00 MHz focused transducer without filtering. Figure 22 shows a typical nonfiltering output y(t) for this transducer. Figures 23 and 24 show the input and output received respectively of the 1.00 MHz transducer with the sample filter applied to the signal. Both outputs were for Model 1. The output signals for Model 2 had waveforms spaced closer together and the signals from the other transducers had a different base frequency, but all inputs and outputs were of similar nature.

Figures 25, 26, and 27 show the input frequency spectrum X(f) for the 2.25 MHz focused, 2.25 MHz unfocused, and 1.00 MHz focused transducers respectively. These plots show that the majority of the signal energy is found in a region about the center frequency of the transducer. This demonstrates the band-limited nature of the signal and

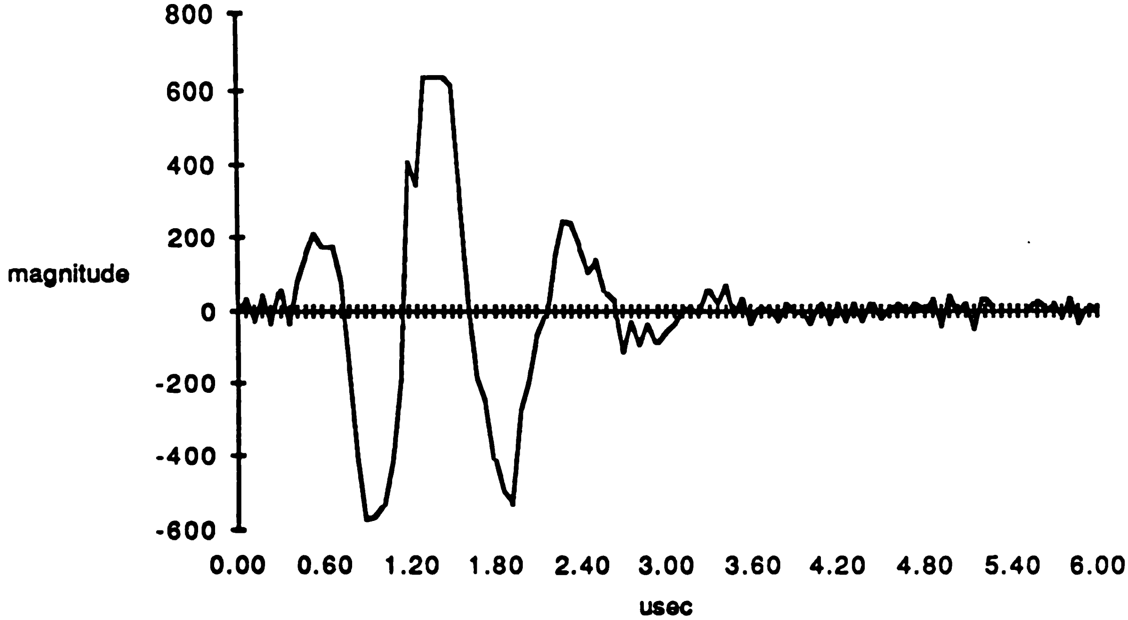

Figure 21: Typical Input: 1.00 MHz, Focused, Nonfiltered

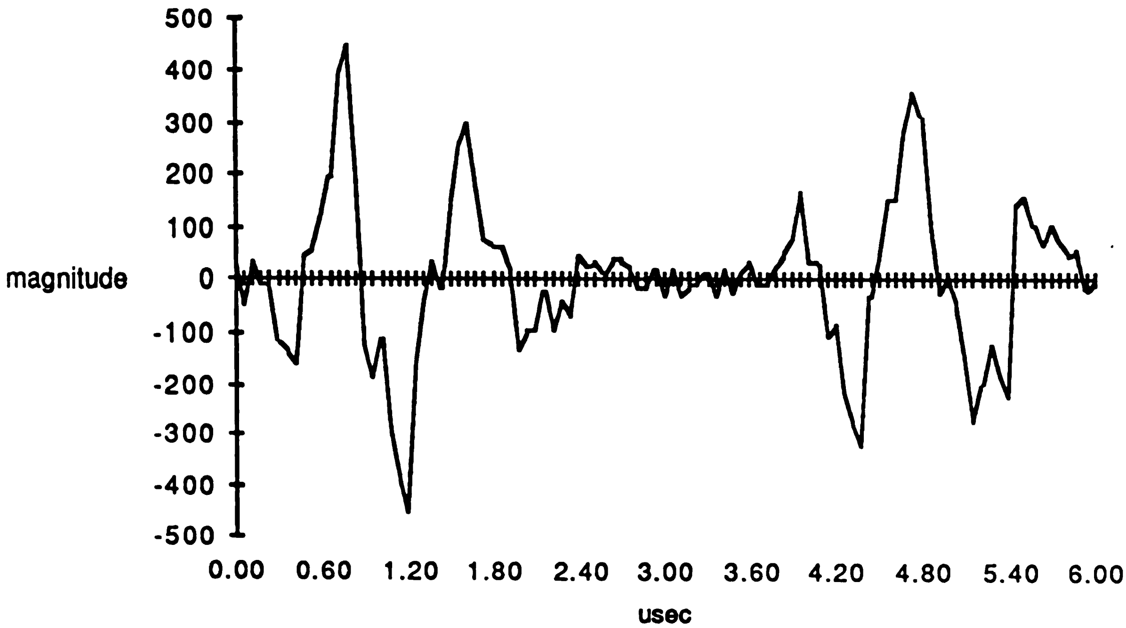

Figure 22: Typical Output: 1.00 MHz, Focused, Nonfiltered

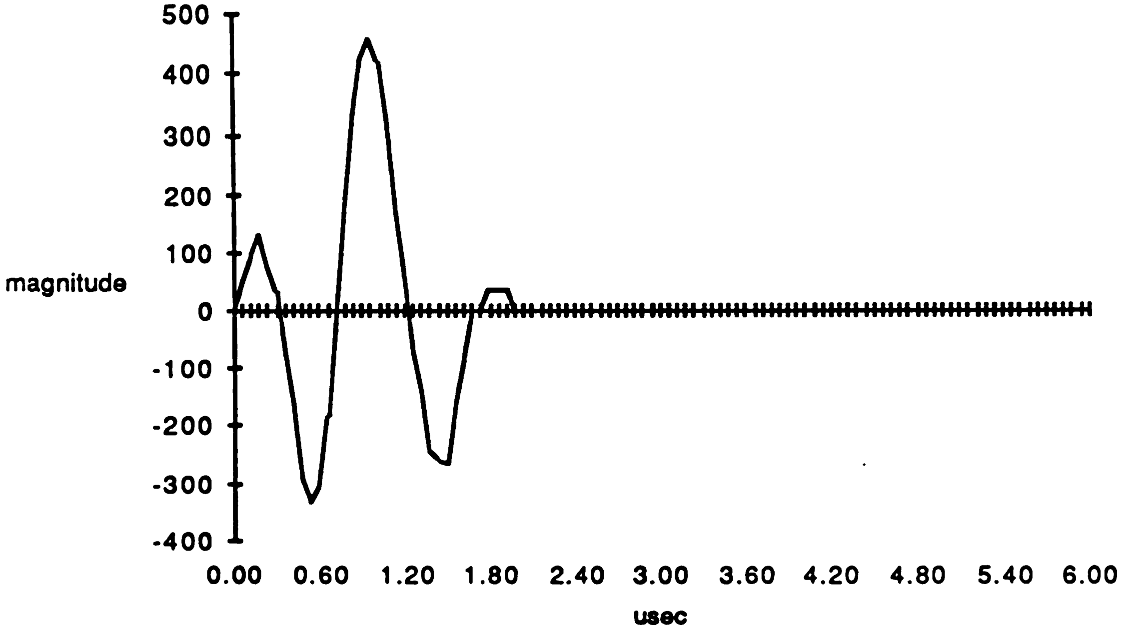

Figure 23: Typical Input: 100 MHz, Focused, Filtered

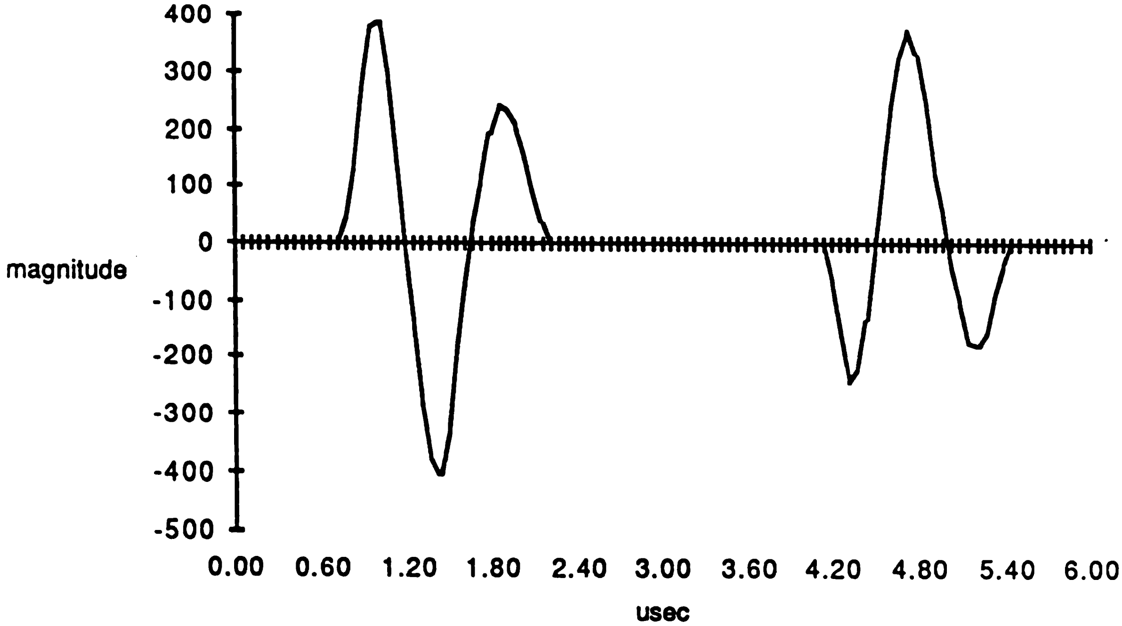

Figure 24: Typical Output: 1.00 MHz, Focused, Filtered

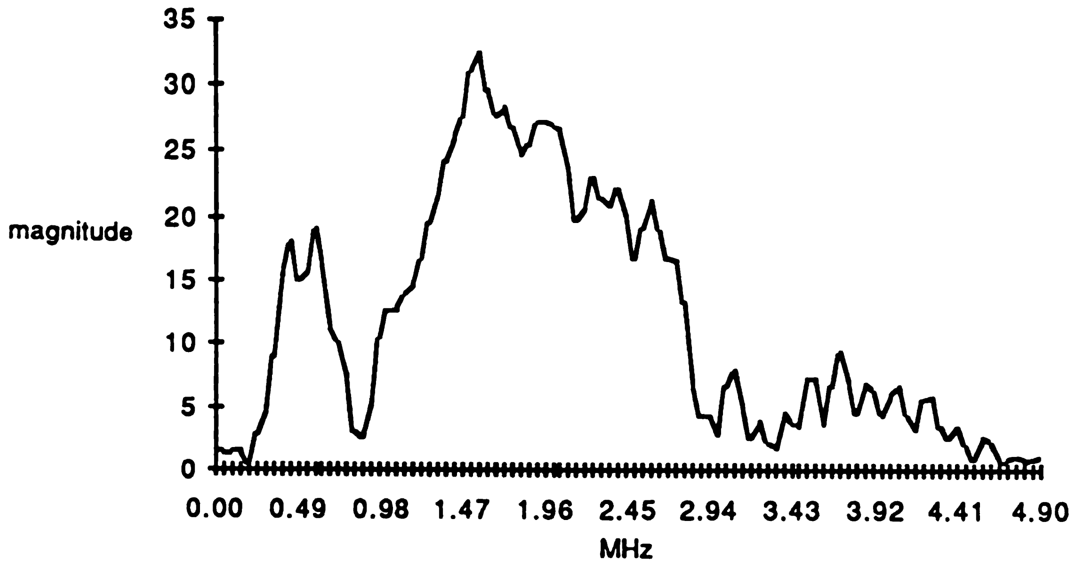

Figure 25: X(f) for 2.25 MHz, Focused Transducer

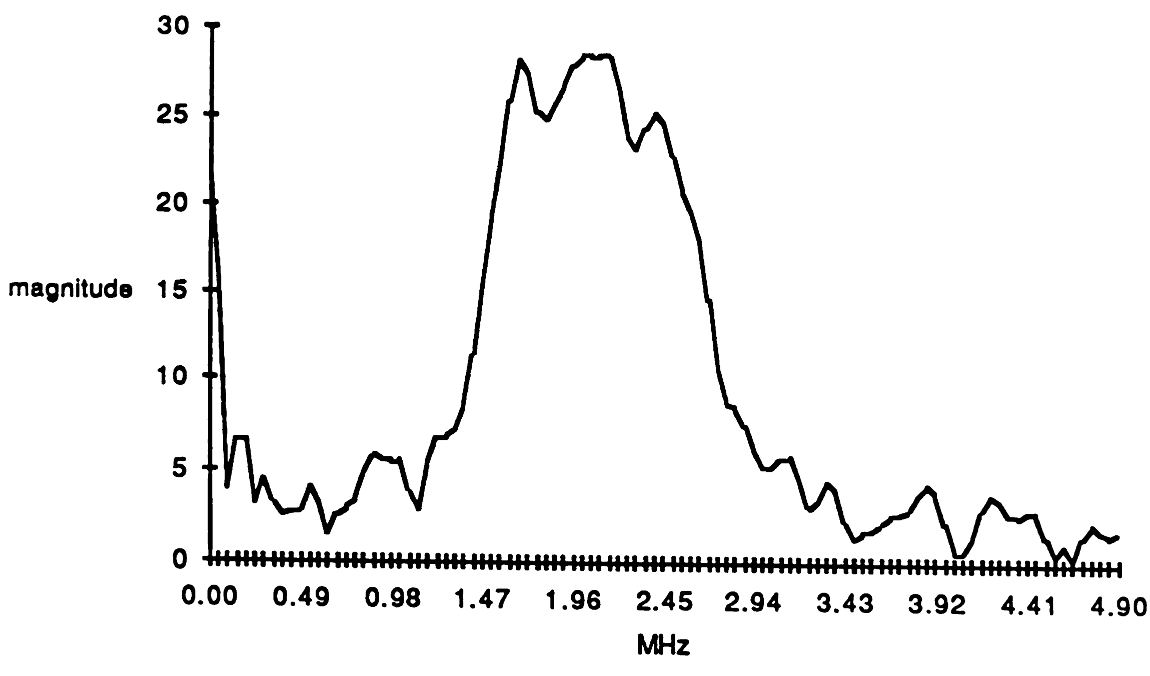

Figure 26: X(f) for 2.25 MHz, Unfocused Transducer

justifies the use of a windowing filter discussed in Section 2d. Figure 28 shows the output spectrum Y(f) for the 1.00 MHz transducer interrogating Model 1 (Trial 1). The spectrum shows that again the majority of the energy is contained in a band about the center frequency. The major difference between X(f) and Y(f) is that the output spectrum has an oscillatory spectrum imposed on it. This effect is called scalloping. When Y(f) is divided by X(f), this oscillatory spectrum should come out giving a spectrum similar to the spectrum of an ideal impulse response (Figure 8).

Figures 29 through 52 present the impulse response frequency spectrum H(f) and the impulse h(t) for twelve different trials. Due to variability in the range gate setting and in the mounting of the transducer in the model, the impulse responses were framed so that the first reflection always occurred at 0.60 usec. The speed of sound in acrylic is approximately 1660 m/sec, so for Model 1 (6 mm of acrylic) the second echo should have occurred at 4.2 usec and for Model 2 (1 mm of acrylic) the echo should have occurred at 1.2 usec. The impulse responses were judged by two criteria. First is the ability to observe two distinct peaks in the impulse response that corresponds to the two boundaries. The second criteria was if the location of the peaks in h(t) corresponded to the

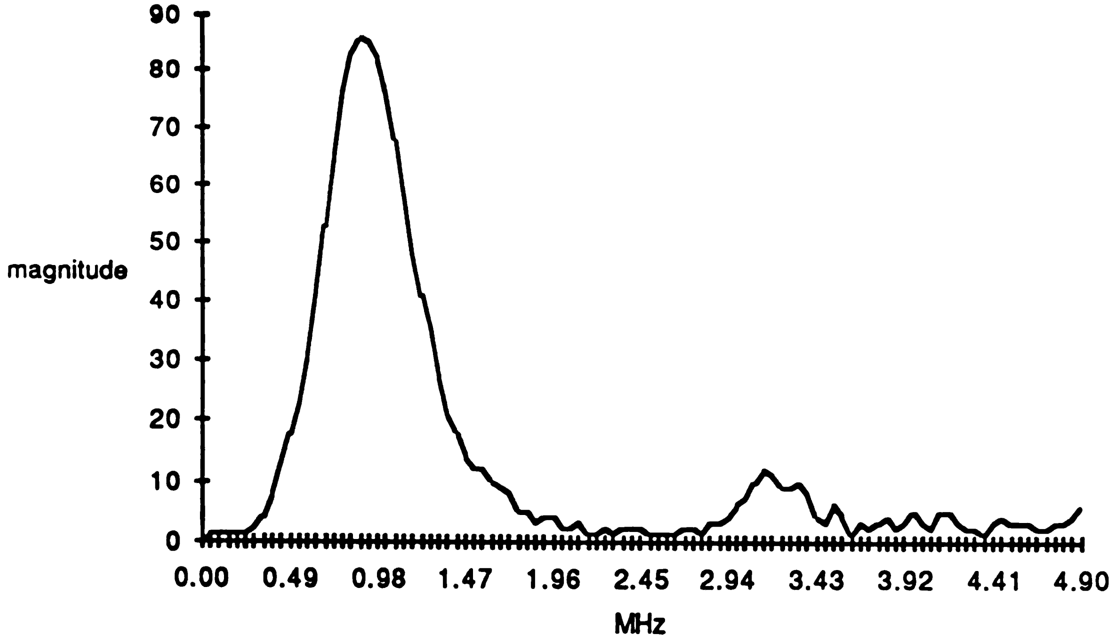

Figure 27: X(f) for 1.00 MHz, Focused Transducer

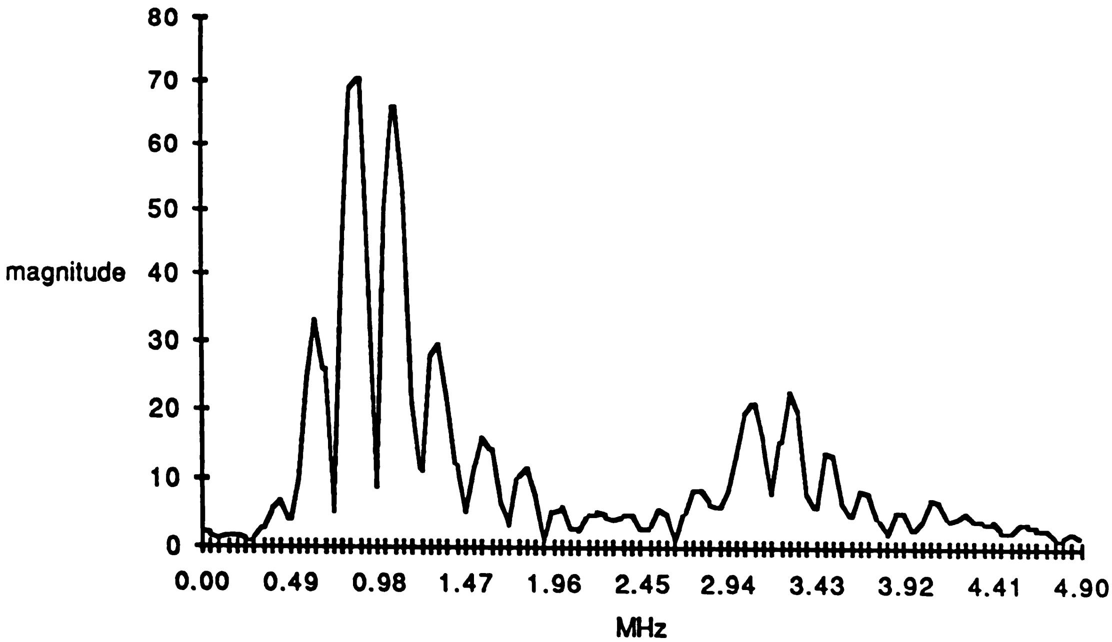

Figure 28: Y(f) for Trial 1

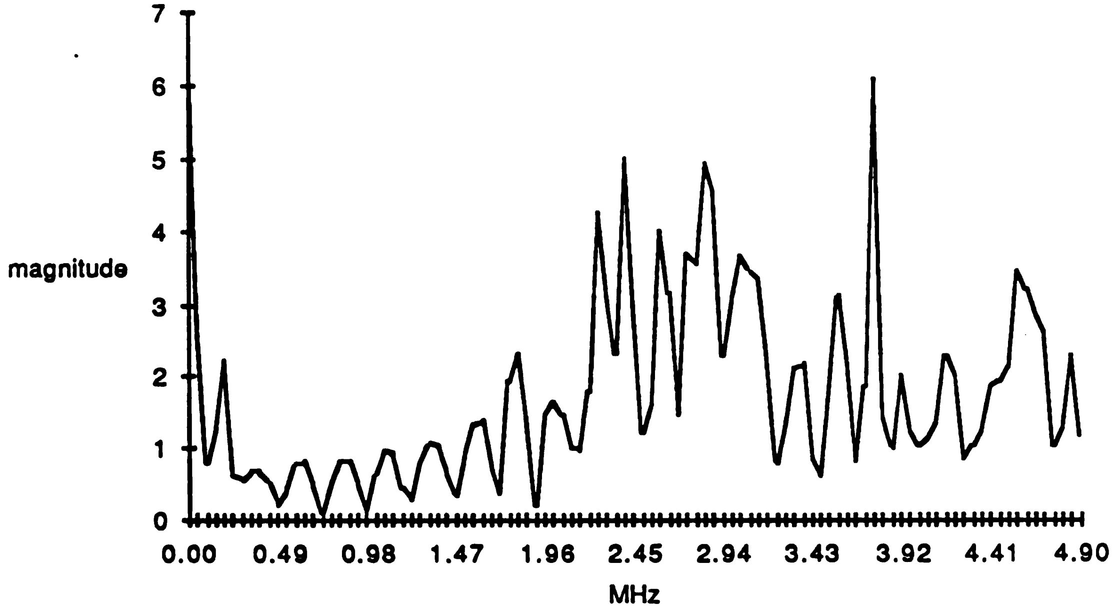

Figure 29: H(f) for Trial 1

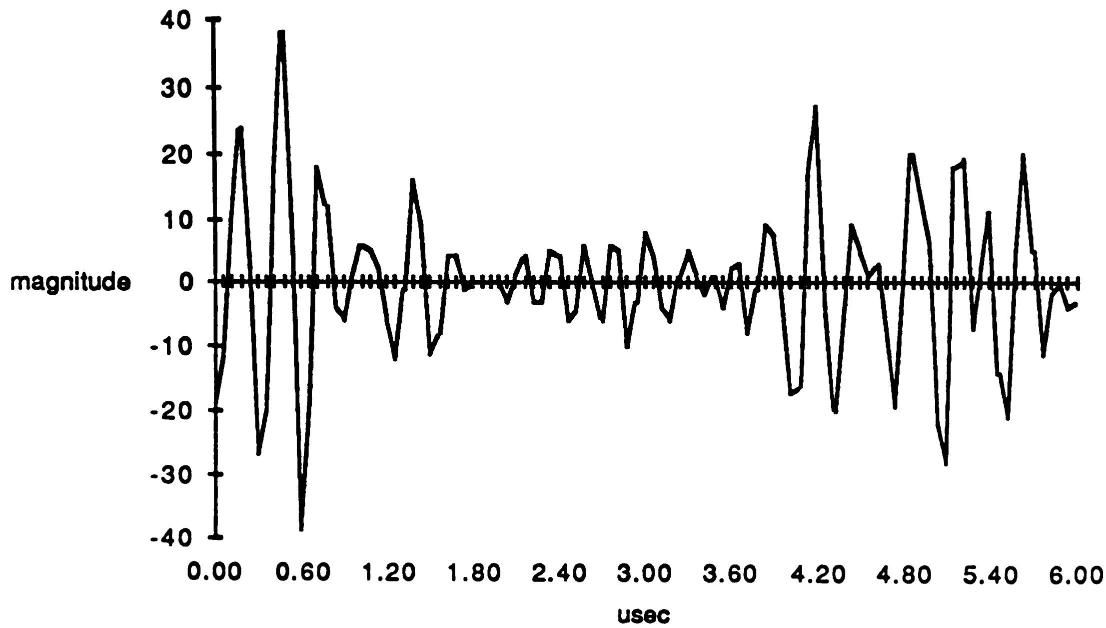

Figure 20: h(t) for Trial 1

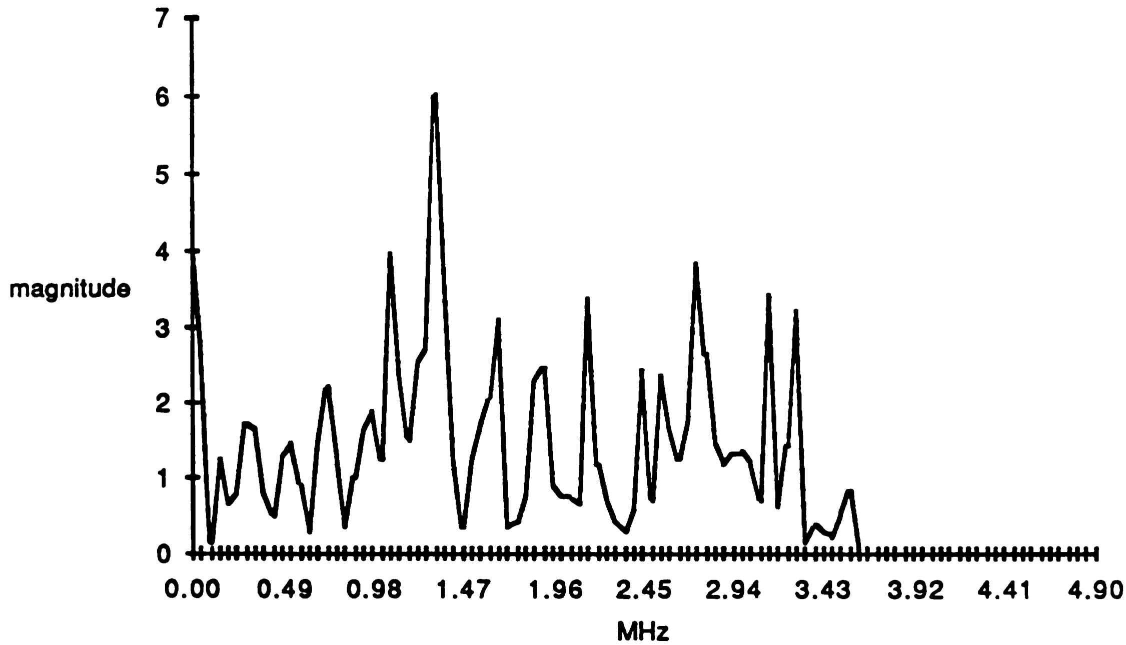

Figure 31: H(f) for Trial 2

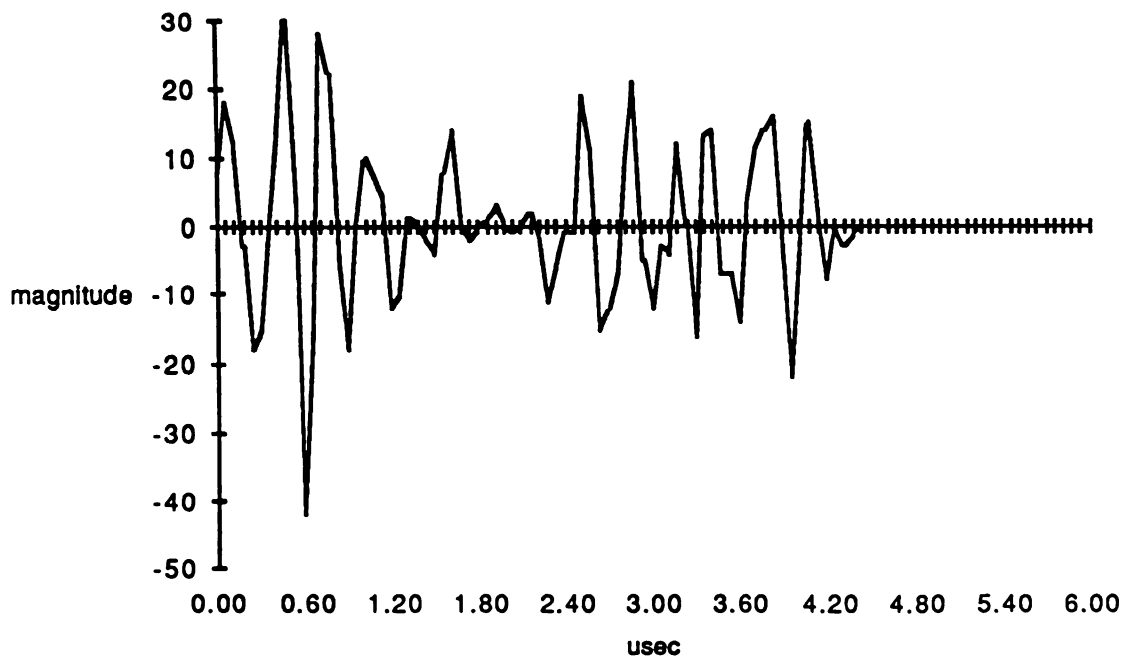

Figure 32: h(t) for Trial 2

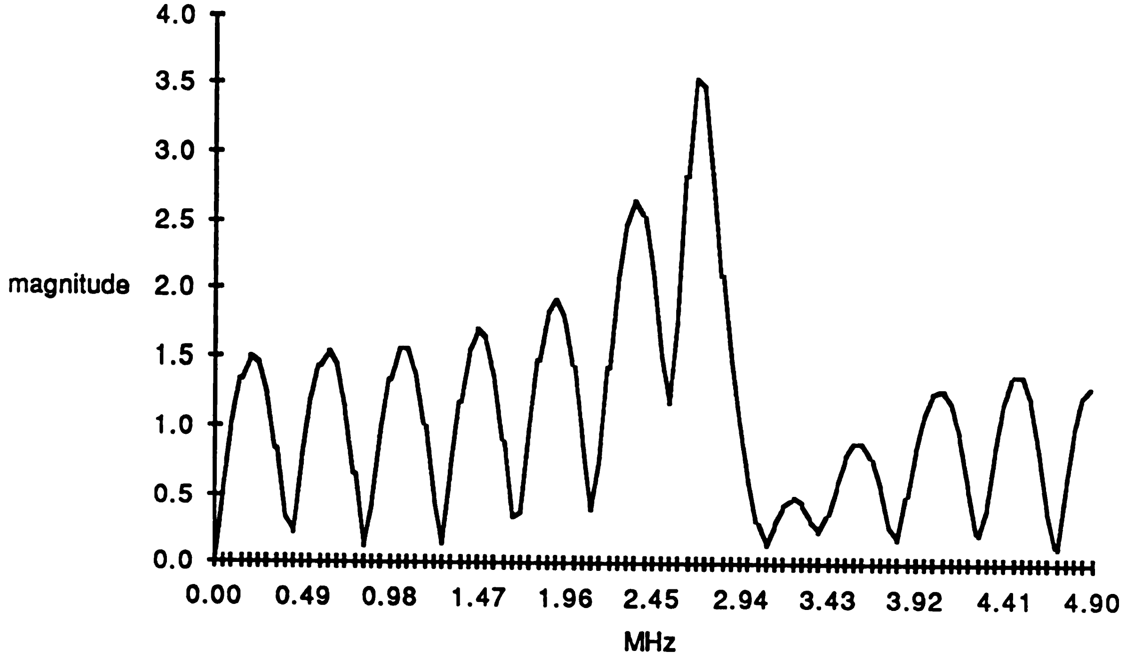

Figure 33: H(f) for Trial 3

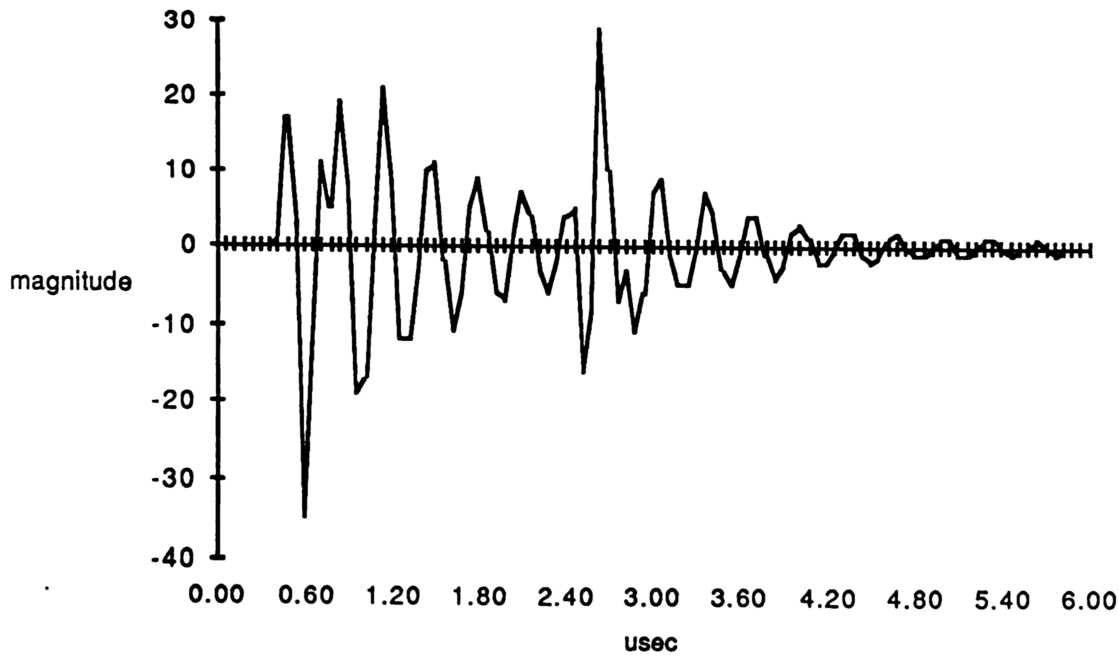

Figure 34: h(f) for Trial 3

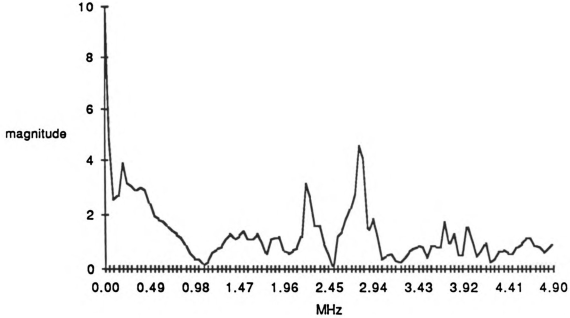

Figure 35: H(f) for Trial 4

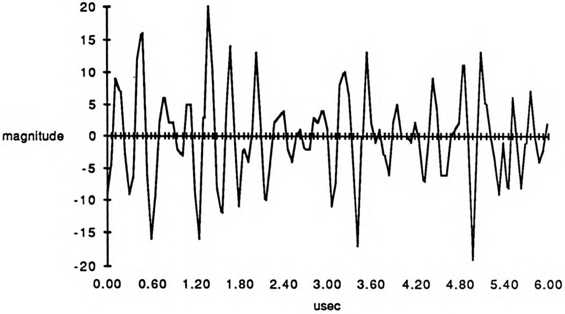

Figure 36: h(t) for Trial 4

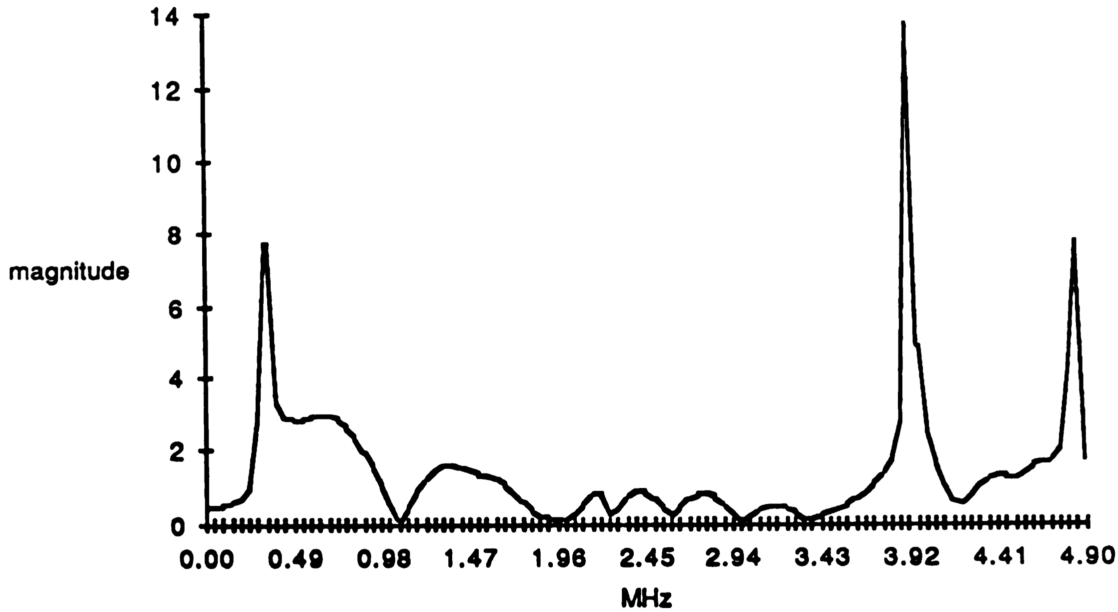

Figure 37: H(f) for Trial 5

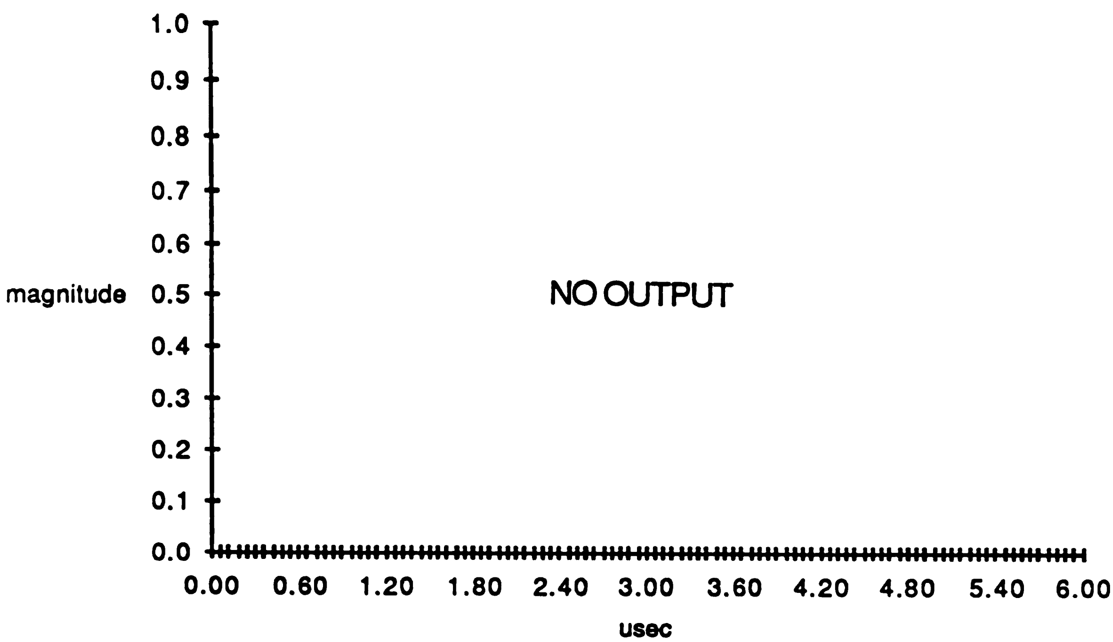

Figure 38: h(t) for Trial 5

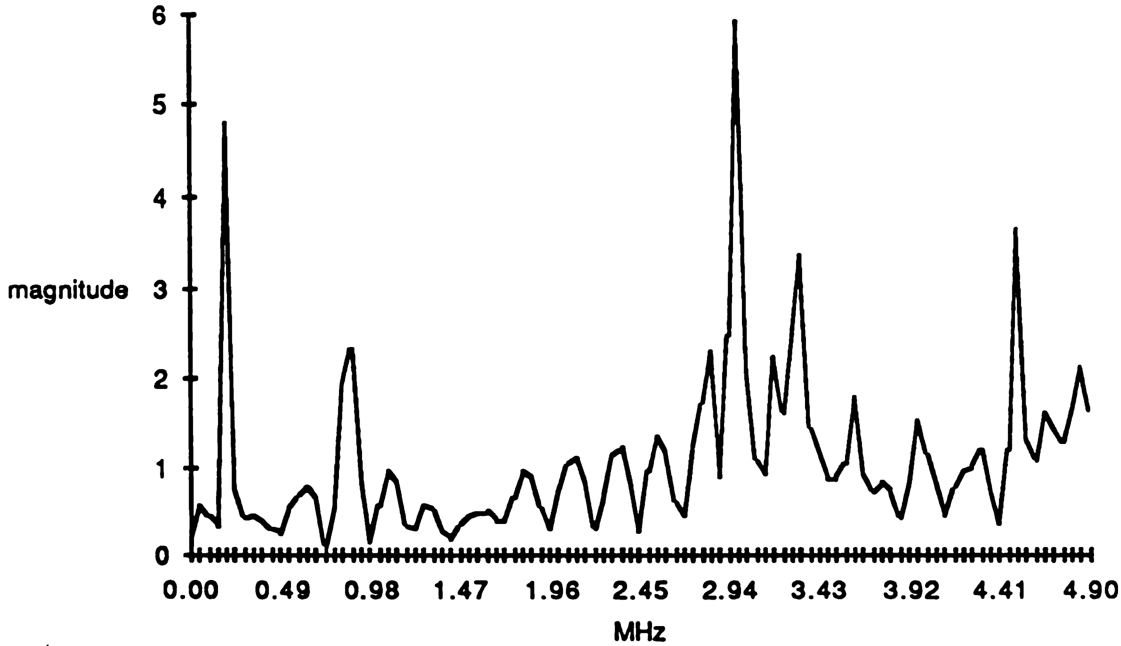

Figure 39: H(f) for Trial 6

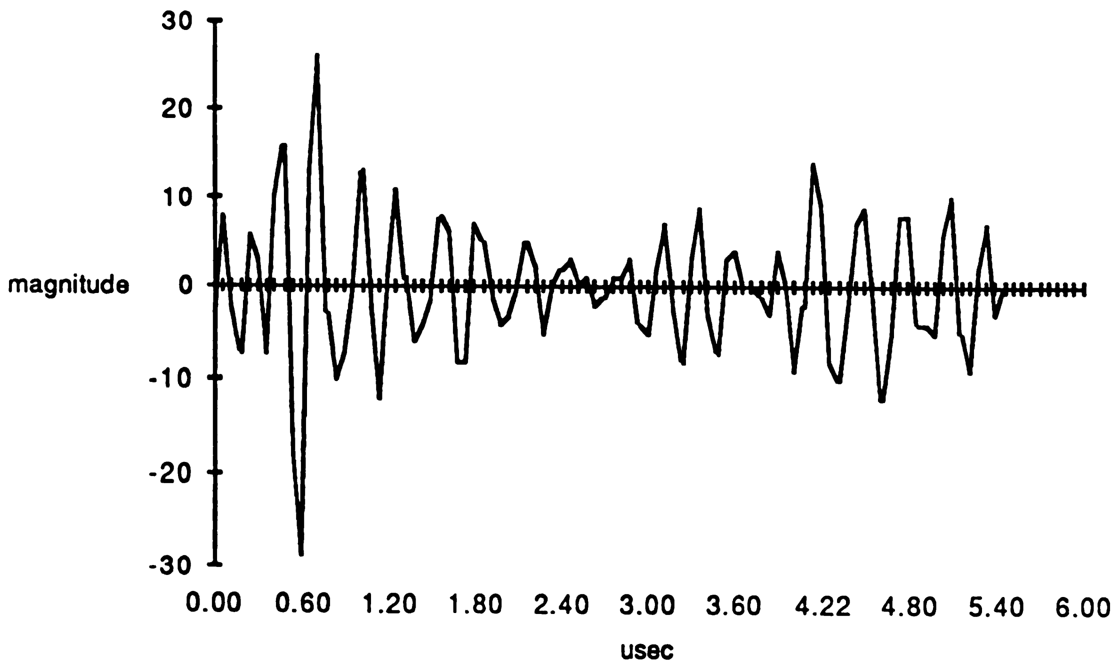

Figure 40: h(t) for Trial 6

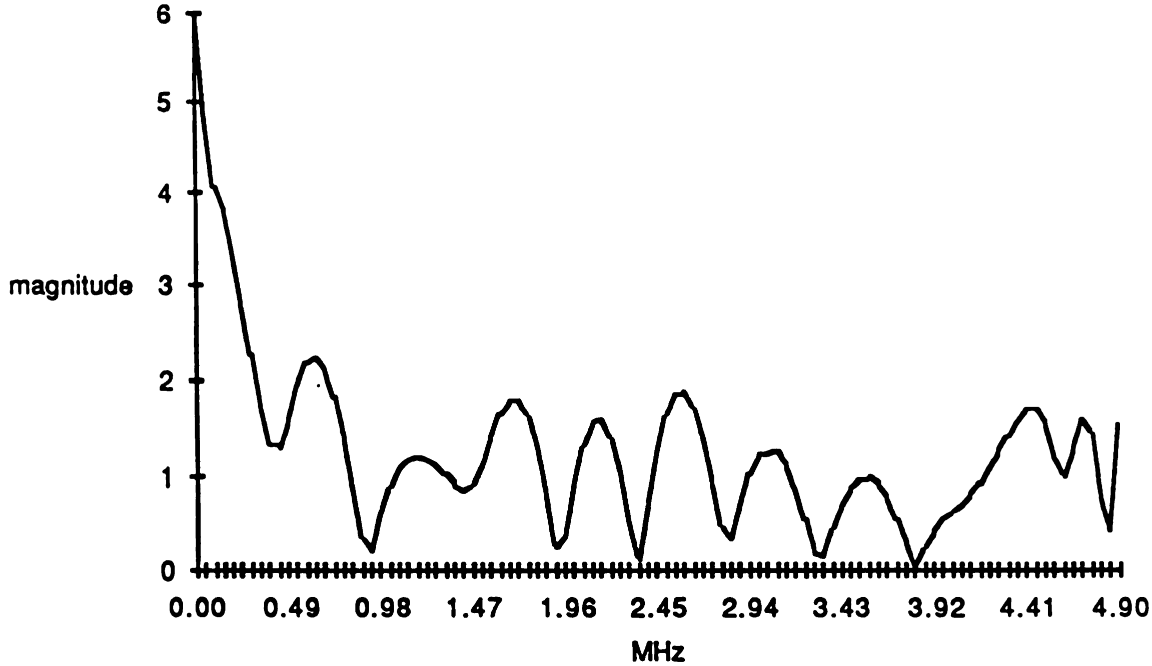

Figure 41: H(f) for Trial 7

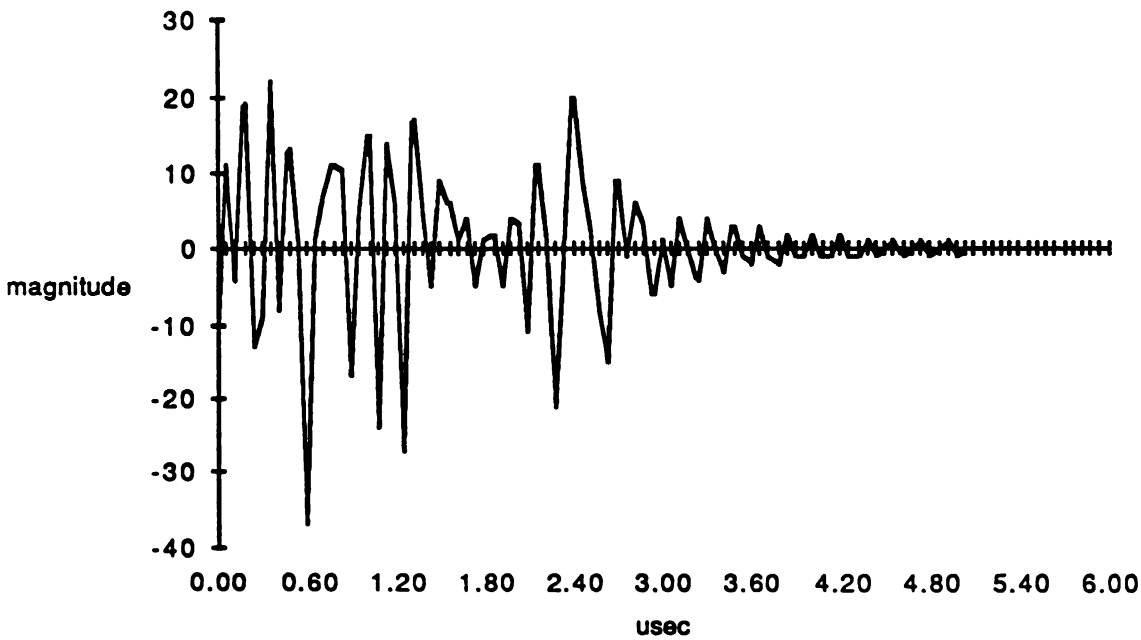

Figure 42: h(t) for Trial 7

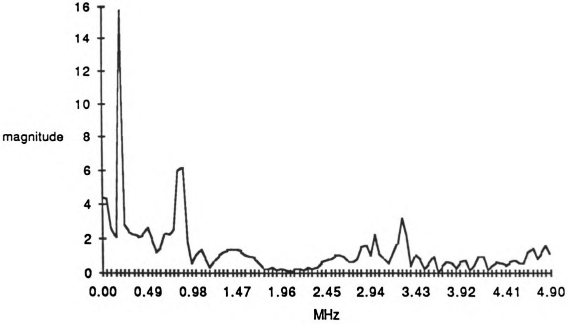

Figure 43: H(f) for Trial 8

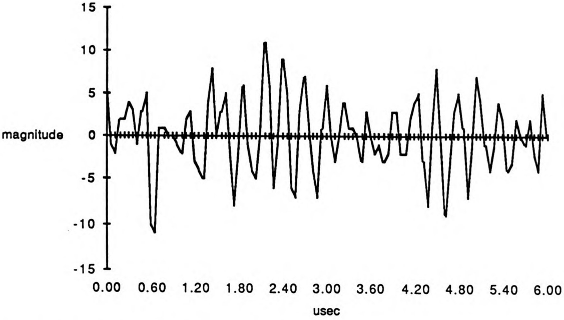

Figure 44: h(t) for Trial 8

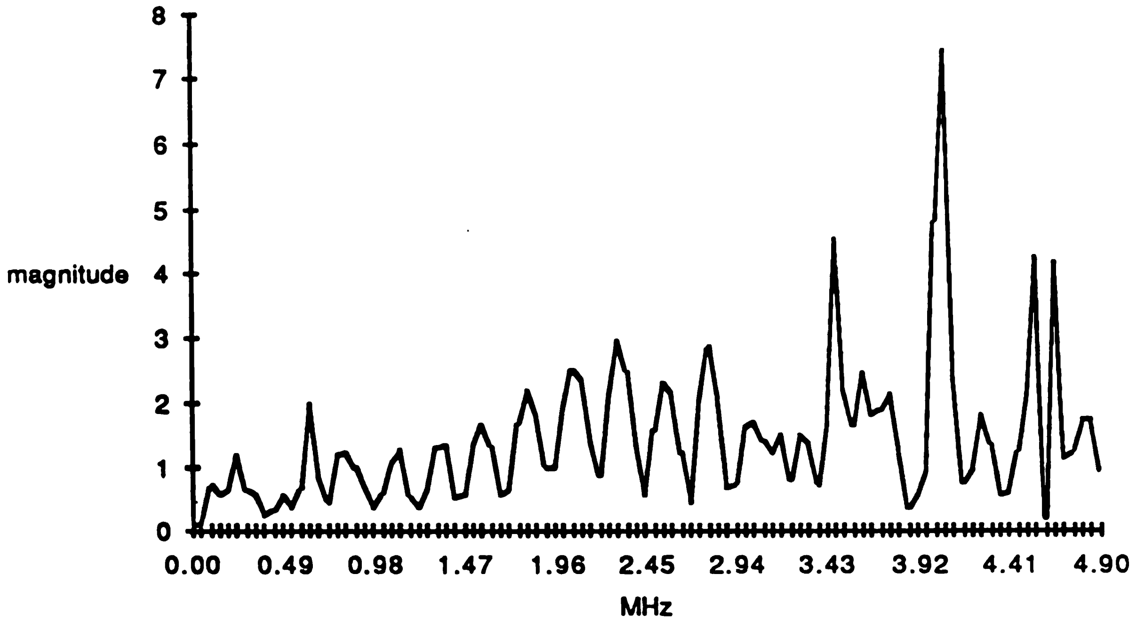

Figure 45: H(f) for Trial 9

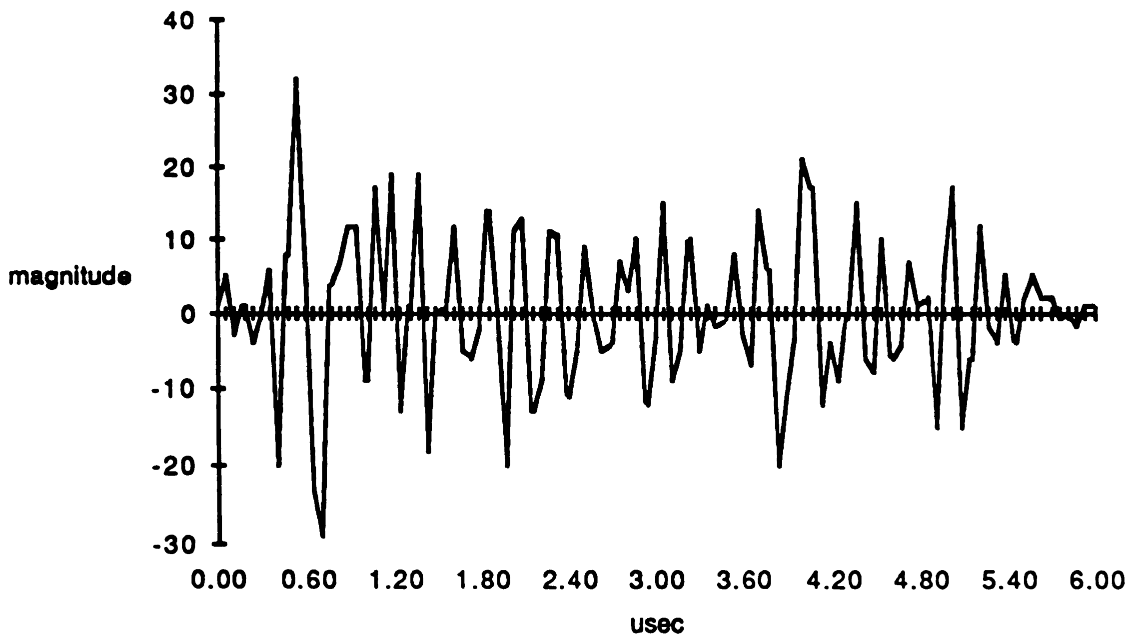

Figure 46: h(t) for Trial 9

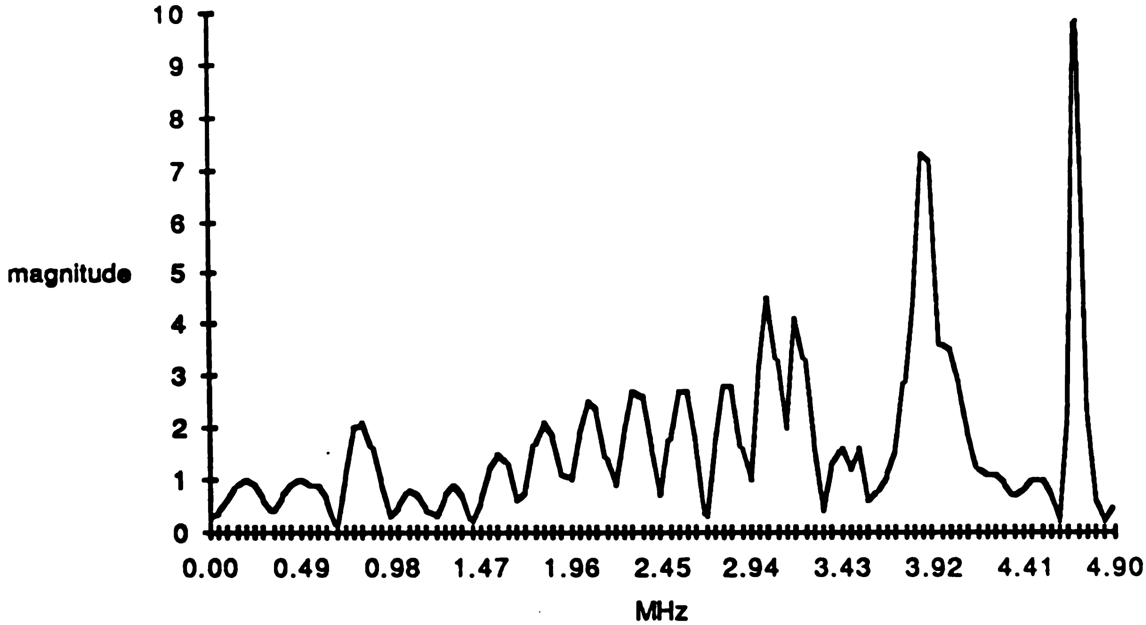

Figure 47: H(f) for Trial 10

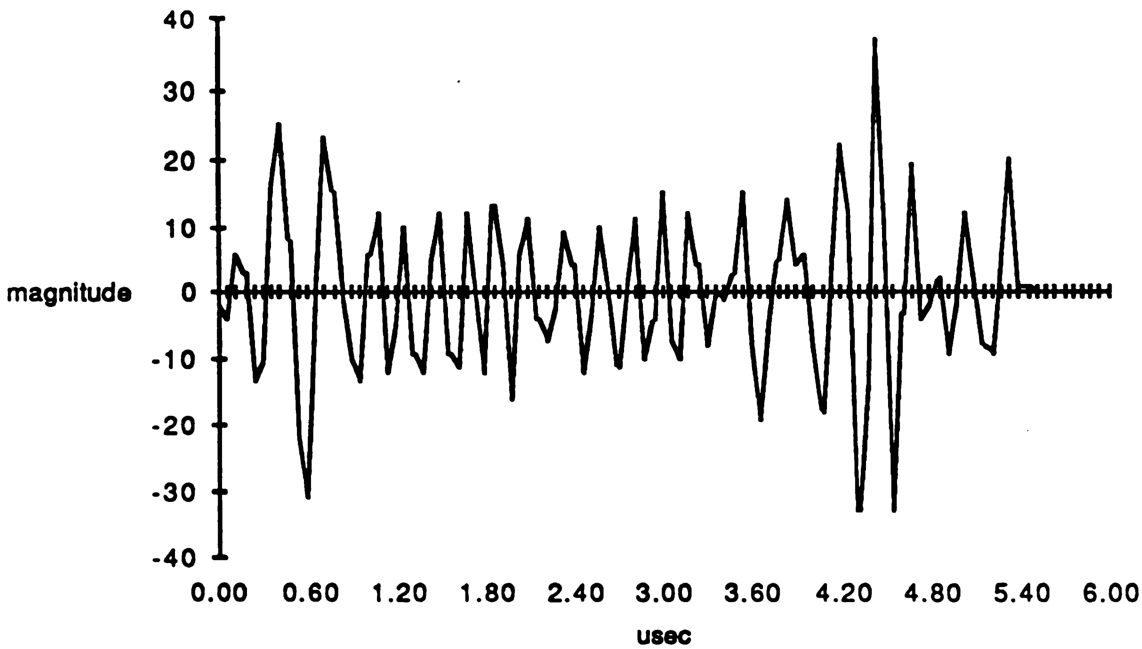

Figure 48: h(t) for Trial 10

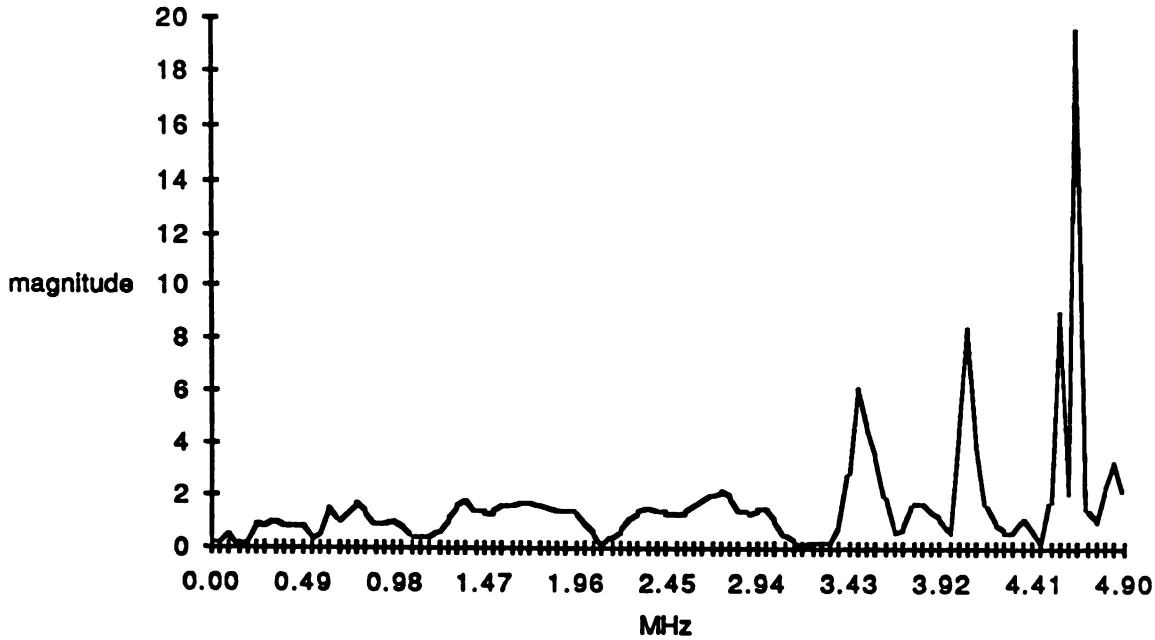

Figure 49: H(f) for Trial 11

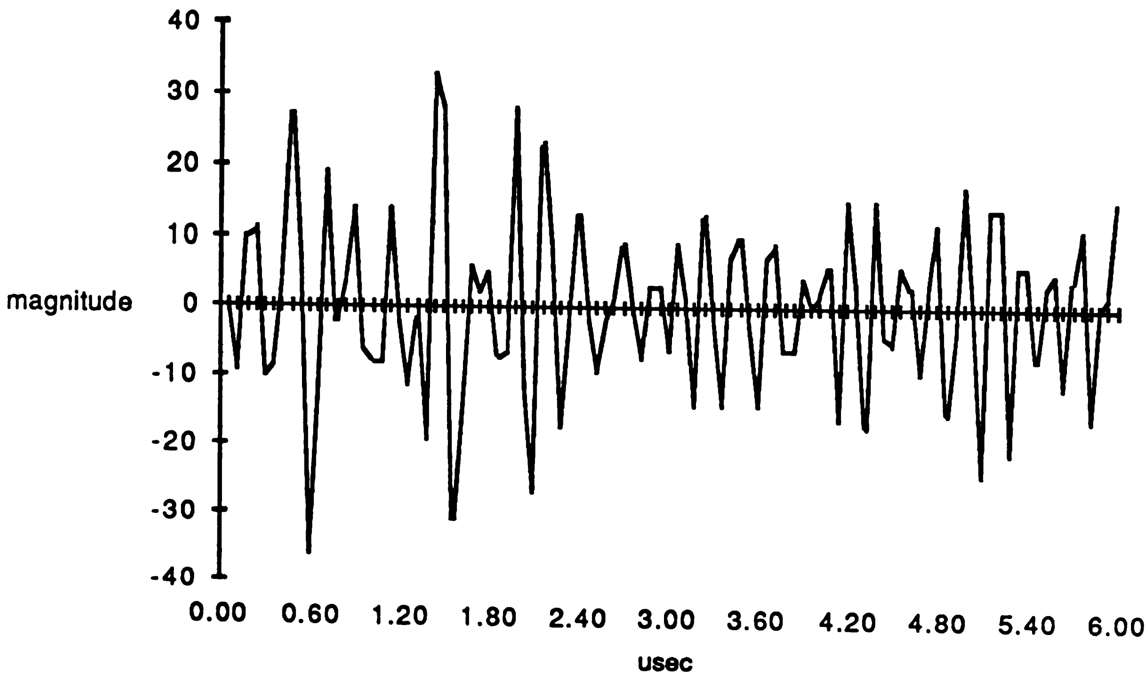

Figure 50: h(t) for Trial 11

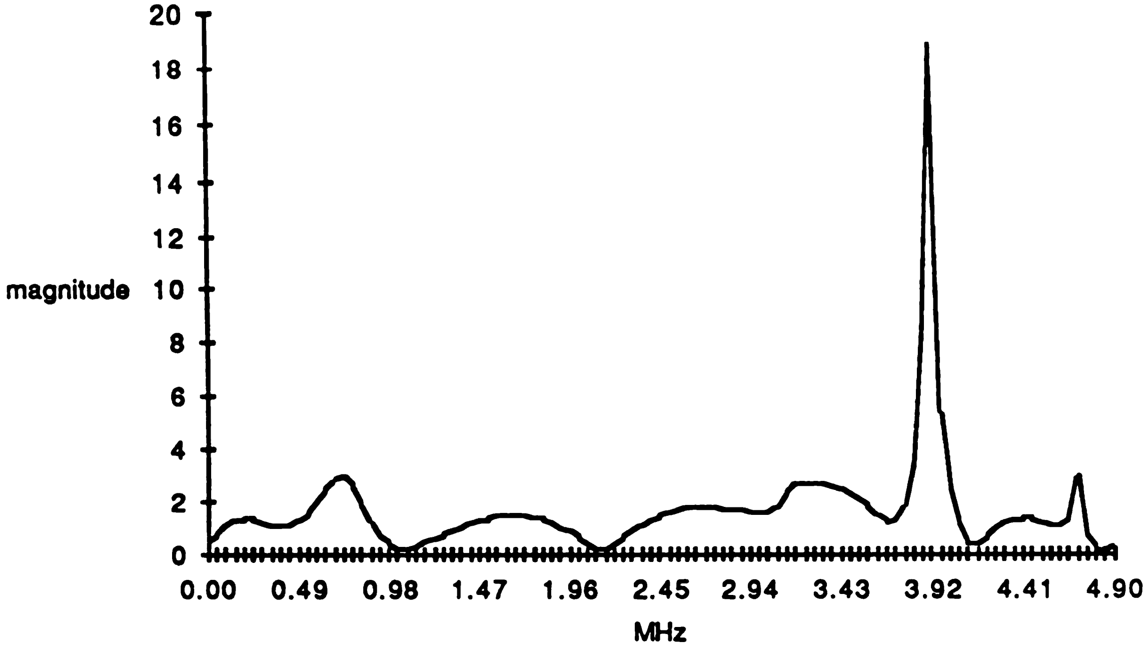

Figure 51: H(f) for Trial 12

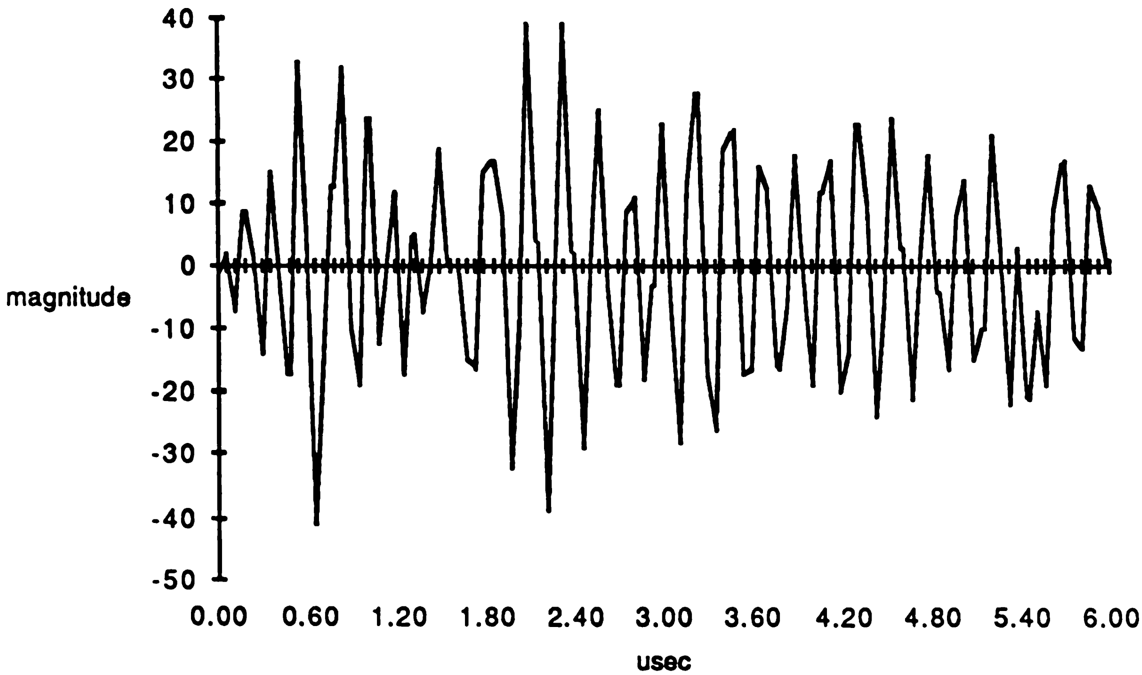

Figure 52: h(t) for Trial 12

anticipated location in time. Table 1 summarizes the trial parameters and the results.

TABLE 1: SUMMARY OF RESULTS

Trial #	TRANSDUCER	MODEL	FILTER	RESULTS	FIGURES
1	1.00 focused	1	none	good	29, 30
2	1.00 focused	1	simple	poor	31, 32
3	1.00 focused	1	single peak	good	33, 34
4	1.00 focused	2	none	good	35, 36
5	1.00 focused	2	simple	unstable	37, 38
6	2.25 focused	1	none	good	39, 40
7	2.25 focused	1	simple	fair	41, 42
8	2.25 focused	2	none	poor	43, 44
9	2.25 unfocused	1	none	fair	45, 46
10	2.25 unfocused	1	simple	good	47, 48
11	2.25 unfocused	2	none	good	49, 50
12	2.25 unfocused	2	simple	poor	51, 52

There are several general observable trends. First, the impulse response method improves resolution. The theoretical limit of resolution of an envelope-detected signal is the wavelength of the signal. For a 1.00 MHz signal in acrylic this is 1.6 mm. Figure 36 clearly shows two boundaries .6 usec or 1 mm apart. The second trend was that the frequency of the transducer did not seem to make much difference. If there were any advantages, it would have been the 1.00 MHz transducer, as more of its signal was contained in the bandwidth of the system. The two focused transducers seem to have given a more accurate measure of distance than the unfocused transducer. Trials 9, 11, and 12 show an error in the location of the boundaries. A possible explanation for this could be multiple reflection paths observed by the transducer due to the dispersity of the unfocused beam. Finally, and probably most surprisingly, the simple filter and threshold detection had an adverse effect in most cases. The nonfiltered signals probably worked adequately because noise components canceled each other out when taking H(f). The filter and threshold detector could have caused the unstable transformer in Trial 5 and degraded the signal enough to change the impulse response. The exception to this was the single peak detection, but this scheme is difficult to implement automatically while preserving the signal.

4d. Future Possibilities

This thesis has pointed to the possibilities of using the impulse response to find both the impedance and attenuation profiles. Thus the obvious next step is to do this. Although the system did a reasonably good job of finding boundaries in the impulse response, there will be a problem in finding the impedance and attenuation profiles for two reasons. First, the noise level in non-boundary regions is significant. This will tend to produce noise in the profiles. Secondly, the impulse response at the boundary is not always a single peak, but a series of positive and negative peaks. This effect will also corrupt the profile.

There are several approaches that could be taken to alleviate these problems. The easiest way to improve the profile would be to write a sorting program that would detect peaks that are truly part of the impulse response, and ignore those created by noise and bandwidth limitations. Another way to increase the accuracy of the impulse response would be to increase the sampling frequency. The present rate of 14.67 MHz could be increased to the system limit of 20 MHz. The system would then record the wave form in more detail and give better results. In theory this would improve the resolution of the system. One final way to improve the system is to explore different signal processing schemes. The present ones were chosen because of their simplicity. The two most obvious avenues to explore would be the actual acquisition filter and threshold detection. The other would be to perform the iterative techniques on H(f) to restore frequencies outside the range f1,f2.

There is work to be done before impedance and attenuation imaging are practical. The automated system for determining the impulse response performed well in finding the impulse response of the models. This system is a step closer to that realization.

APPENDICES

APPENDIX A

APPENDIX A

FOURIER TRANSFORMER

The Fourier transformer used to calculate the impulse response for this thesis was performed on Michigan State University Cyber 750. The specific routine used was the FFTCC. This routine is resident in the Hustler Auxiliary Library and will take the fast Fourier transformer of a complex waveform and return a complex waveform. The number of samples used in the transform was 296, whereas the number of samples used from the signal was 120. All other points were set to zero. This gave an impulse response of 148 usable points (the other 148 are mirror points from the transform). If a wider range of observation is desired both the number of samples and the number used in the transform will have to be increased.

APPENDIX B

APPENDIX B

ALGORITHM FOR REDUCING NOISE COMPONENTS FROM SPECTRUM

The following process was used to try to eliminate the noise from the spectrum of the impulse response H(f). First the notation used

$H(f)$ = the actual spectrum of the impulse response

$H_o(f)$ = the spectrum of the impulse response plus noise

$N(f)$ = the spectrum of the noise

$W(f)$ = windowing function used

$H'(f)$ = estimate of the actual spectrum

The process:

1. Obtain $H_o(f)$ by dividing $Y(f)$ by $X(f)$

2. Calculate the window function $W(f)$ given by

   $$W = \cos^2 \frac{\pi(i - i_0)}{2\Delta i} \quad \text{for } i_0 - \Delta i < i < i_0 + \Delta i \text{ and } N + 2 - i_0 - \Delta i < i < N + 2 - i_0 - \Delta i$$

   $$W = 0 \qquad \text{otherwise}$$

   where i_o is the center frequency of the incident signal spectrum and i is its bandwidth

3. calculate $H'(f)$ by $H'(f) = W(f) \cdot H_o(f)$

APPENDIX C

APPENDIX C

SYSTEM SOFTWARE

The system used two different programs run on two different computers. The first was the data acquisition program run on the Cromemco microcomputer. The other program was the signal processing program run on the Cyber 750.

The data acquisition program was written in Basic and its function was to:

1. control the system sampling,
2. read data from system,
3. perform any filtering or threshold detection desired,
4. display digitized signal on CRT for checking,
5. write signal on a floppy disk.

The part of the program that performed steps 1 and 2 was written in Assembly Language and called as a routine by the Basic main program. The filtering in step three took a long time in Basic so this program should be changed to a faster language when the exact filtering scheme is decided.

A utility program was used to transfer the data from the disk to permanent file on the Cyber. The signal processing program then performed the following steps:

1. read the range of the data file to use in the program,
2. read that range of the data files,
3. display or plot $x(t)$ and $y(t)$,
4. calculate $X(f)$ and $Y(f)$,
5. calculate the windowing function $W(f)$,
6. calculate $H(f)$,
7. display or plot $X(f)$, and $H(f)$,
8. calculate $H'(f)=H(f)\ W(f)$,
9. calculate $h(t)$,
10. display or plot $h(t)$.

This program was written in FORTRAN because of the many calculations performed. It can be easily updated to process $h(t)$ and display the impedance profile.

BIBLIOGRAPHY

BIBLIOGRAPHY

Beretsky, I., Farrel, G., "Improvement of Ultrasound Imaging and Medical Characterization by Frequency Domain Deconvolution, Experimental Study with Nonbiological Models," Ultrasound in Medicine, Volume 38, Plenum Press, pp. 1645-1665.

Beretsky, I., Farrel, G., Litchenstein, B. "Raylography, A Pulse Echo Technique with Future Biomedical Applications," Proceedings of the 20th Annual Meeting of the American Institute of Ultrasound in Medicine, pp. 401-409, 1976.

Jayasumana, M.A. "Acoustic Attenuation and Impedance Characterization by Bi-directional Impulse Response Technique," M.S. Thesis, pp. 16-41, Michigan State University Press, 1982.

Jones, J.P., "Impediography: A New Ultrasonic Technique for Diagnostic Medicine," Ultrasound in Medicine, Volume 1, pp. 489-497, Plenum Press, 1974.

Jones, J.P., "Ultrasound Impediography and it's Applications to Tissue Characterization," Recent Advances in Ultrasound in Biomedicine, pp. 131-156, 1977.

Lichtenstein, B., Beretsky, I., Farrel, G., and Winder, A. "A Medium Characterization by the Application of a Deconvolution Technique in an Acoustic Pulse Echo System - Raylography," Ultrasound in Medicine, Vol. 2, pp. 411-425, Plenum Press, 1975.

Papoulisa, A., Beretsky, I., "Improvement of Range Resolution of a Pulse Echo System," Ultrasound in Medicine, Volume 3B, Plenum Press, pp. 1613-1627, 1977.